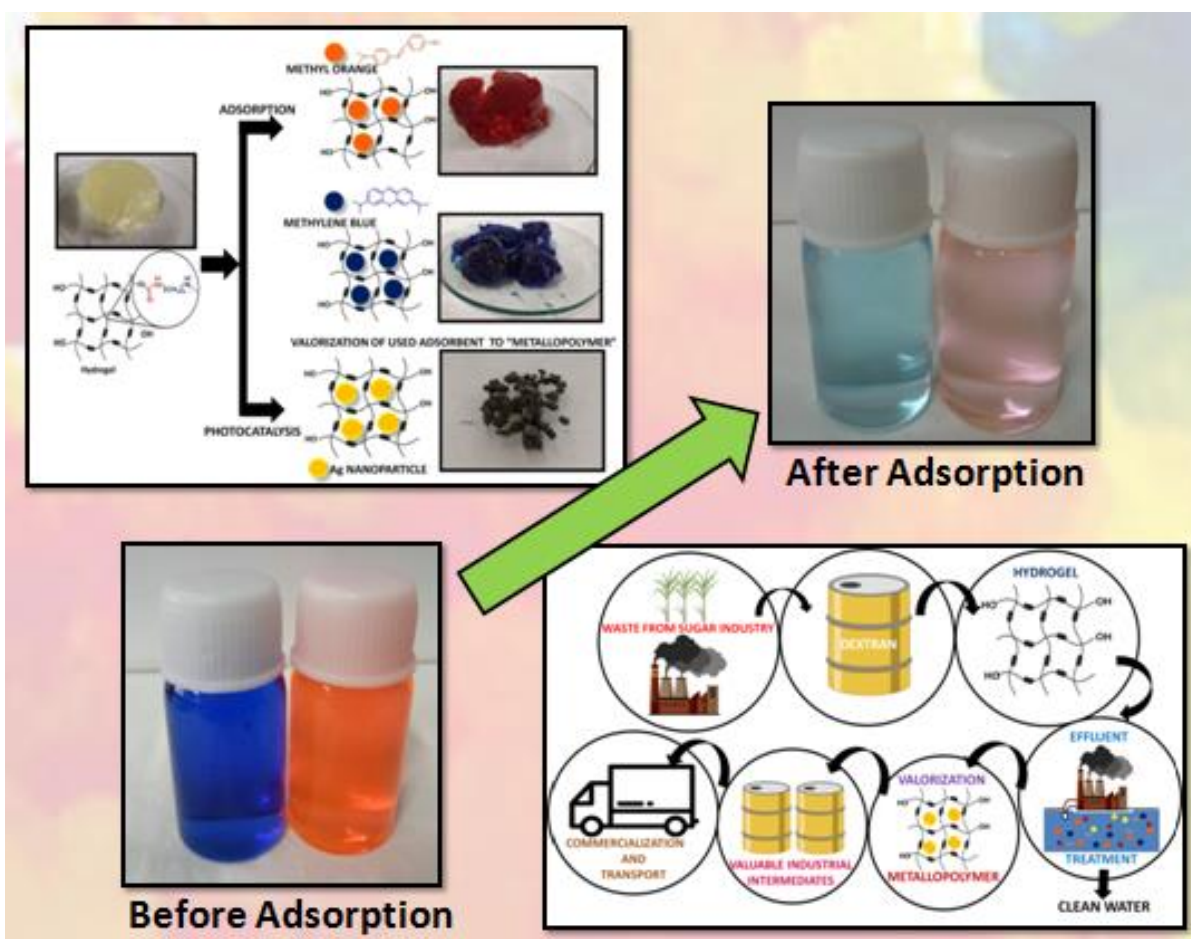


Chapter III

The application of dextran based hydrogel for elimination of organic dyes and reduction of nitrophenols



3.1.Introduction

The sustenance and continuation of life and livelihood require water as a basic necessity. The severe problem faced globally arises due to continuous release of contaminants out of anthropogenic activities pollute the basic quality of water¹. The variation from recommended water quality index makes water unfit for use that degrades health of plants, animals and humans as well as hinder the economic development of the country. The spreading of pollutants has been accompanied by air or water leading to severe environmental as well as health issues all over the world. The effluents released by industries and other sources include both organic and inorganic contaminants. Focusing on organic pollutants; they are mostly human generated and widely used in industrial solvents, many fuel components and intermediates. Organic compounds are categorized according to their molecular structure and functional groups. The group of esters, ketones, amines, acids, ethers, alcohols, hydroxyl etc. can determine the properties of organic compounds. Several listed manufactured products like gasoline, adhesives, plastics, paints etc. contain several detrimental organic compounds². Out of several harmful pollutants, the elimination of dyes and phenolic compounds require attention. Trace amounts of dye pollutants released from printing, dyeing, textile and chemical industries can also cause severe adverse impact on drinking water quality³. The toxic and carcinogenic, mutagenic contaminants are harmful for living beings and environment^{4,5}. On the other hand, the effluents of pharmaceutical industries, oil refineries and petrochemical plants⁶ contains nitrophenols that can cause risk of kidney and liver damage⁷. In order to eliminate these harmful pollutants from environment, several biological, physical and chemical methods were considered such as irradiation, adsorption, membrane process, ozonation, oxidation, ionic exchange, electrocoagulation and coagulation-flocculation^{8,9}. Some of the above mentioned methods are effective but expensive chemicals, potential of bioaccumulation and costly technologies are some significant shortcoming¹⁰. One of the most considerable, convenient and cost-effective technique is adsorption utilized for treatment of effluent resolving the shortcomings of other methods¹¹. Some of the reported adsorbents utilized for pollutant removal with better adsorption properties are MCM¹², graphene oxide³, activated carbon¹³, dendrimers¹⁴, mesoporous SiO₂¹⁵, polymer-clay¹⁶, carbon nanotubes¹⁷, agricultural wastes¹⁸, alumina¹⁹, nano-adsorbent²⁰, hydrogels²¹ and bio-adsorbents²². Among all these adsorbents, hydrogels are composed of three-dimensional network of hydrophilic polymers exhibiting high adsorption capacities based on controllable swelling

property as well as high tendency to hold water with maintained structure²³. However, the studies are generally focused on removal of single pollutant accumulating the utilization cost and limiting the industrial applications¹⁸. Additionally, they possess the disposal and recycling problems associated with already recycled adsorbents. The transformation of such materials into value added products may address the problems associated with regenerated adsorbents. There are only few reports available considering the valorization of adsorbed materials and their application in processes of commercial and industrial importance²⁴. For instance, the surface of metal ion adsorbed hydrogel could be reduced to form metal nanoparticles with in-situ approach. The metal nanoparticles entrapped hydrogel matrix forms composites termed as “metallopolymers”²⁵ that can be used as a significant catalytic system for organic transformation of molecules important in industries^{26,27}.

Considering the overview, the rationale of our study contains development of low cost polysaccharide based hydrogel for the treatment of effluent as well as valorization. The eco-friendly, sustainable and economically viable approach was considered while selecting polysaccharide for hydrogel formation over synthetic polymers. Out of various naturally available polysaccharides, dextran was selected as these are the common waste generated from decayed sugarcane being delayed in processing and also during the sugar manufacturing process due to bacterial decomposition^{28, 29}. The utilization of dextran hydrogel in drug delivery system has been reported because of high surface area as well as their capacity to hold guest molecules such as drugs and non-dissociative hydrogel framework^{30,31}. Some reports also suggest the conjugation of dextran based adsorbents with graphene oxides³² and carbon nanotubes³³ like expensive substrates.

Herein we report a single step facile novel approach for surface modification of dextran with crosslinker hexamethylene diisocyanate resulting in excellent adsorbent system for elimination of anionic and cationic dyes Methyl Orange (MO) and Methylene Blue (MB), respectively. The synthesized hydrogel has been characterized by several analytical techniques and their adsorption properties were investigated by various experimental parameters such as dosage variation, concentration variation, temperature and pH variation, regeneration cycle etc. Detail study of adsorption isotherm and kinetics of adsorption process utilizing hydrogel was also carried out. Since, hydrogel is polymeric in nature, with several hydroxyl groups, therefore; they can also act as effective capping agents for the elimination of heavy metals from contaminated

water. The sunlight- induces photocatalysis in aqueous phase provide motivation for exploring photocatalytic degradation of 4-Nitrophenol using catalyst (Ag entrapped metallopolymer i.e. Ag@Hydrogel) to reduce the toxic and hazardous nitroaromatics from water. This approach has significant potential of adsorbent waste management after remediation as well as its further valorization.

3.2. Materials and Methods

3.2.1. Materials

Dextran (mol. Wt. 6000), hexamethylene diisocyanate (HMDI), dibutyltin dilaurate (DBDTL) and acetone were purchased from Sigma Aldrich, India. Methylene blue (MB) and Methyl orange (MO) were obtained from Fisher Scientific, Navi Mumbai, and Laboratory Sulab Reagent, Baroda, India. N, N-Dimethylformamide (DMF) was purchased from Qualigens, Mumbai, India. HCl, NaOH and NaCl were procured from SRL, India. Other reagents were of analytical grade, purchased from commercial sources. All the chemical and reagents were used as received without further purification. The solutions of dyes were prepared using de-ionized water.

3.2.2. Synthesis of Hydrogel (DEX-HMDI)

For the synthesis of the hydrogel, dextran (0.5 g) was dissolved in 10 mL of DMF in round bottom flask and kept for stirring in inert atmosphere under nitrogen. HMDI (0.125 mL) was dissolved in 5 mL of DMF; the resultant solution was added to the solution of dextran slowly dropwise under stirring. The resultant clear solution obtained was heated in an oil bath at controlled temperature of 70°C in presence of DBDTL (50 µL) as catalyst represented in **Figure 3.1**. The product (crosslinked polymer) precipitates out from the reaction mixture after 30 min of reaction progression. The product obtained was thoroughly washed with deionized water followed by washing with acetone. The product was dried in a vacuum oven at 40 °C for 8 h and stored under a vacuum for further use in experiments.³⁴ For 0.6 g of dextran, 1.2 g of hydrogel was obtained.

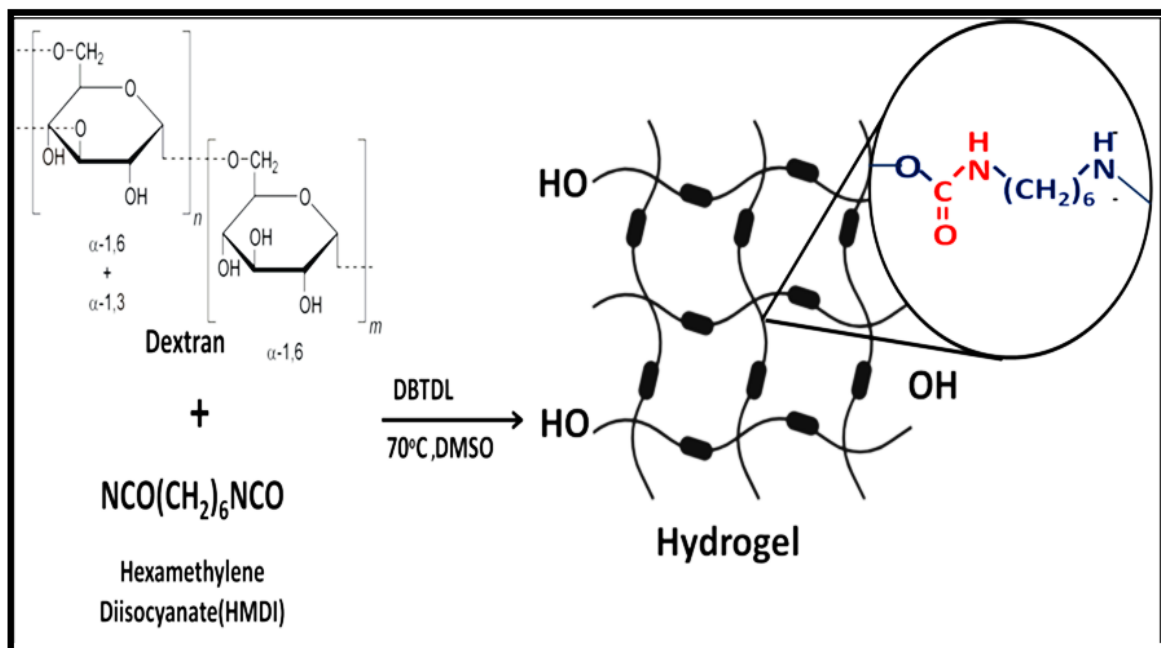


Figure 3.1: Schematic description of process for synthesis of dextran derived Hydrogel

3.2.3. Characterization of DEX-HMDI

The solid state NMR spectrum of the hydrogel (DEX-HMDI) was recorded on JEOL ECZR (600 MHz) NMR spectrophotometer. Fourier Transform Infrared (FTIR) spectra of DEX-HMDI were recorded on Bruker Alpha IR spectrophotometer using KBr discs at room temperature. A JSM-5610 LV model was used to record Energy Dispersive X-ray (EDX) analysis of the vacuum dried hydrogel. The structure of the hydrogel was investigated at room temperature using D2 Phase 2 Bruker X-ray powder diffractometer. X-Rays of wavelength 0.1454 nm (Cu K-alpha) were produced using a tube, a dried and pressed powder of the material was used as sample and diffraction patterns were collected in 0.5 steps per second with 2θ ranging between 10° to 90° . A TG-DTA 6300 INCARP EXSTAR 6000 was used for Thermo Gravimetric Analysis (TGA) under maintained nitrogen atmosphere throughout the measurement at heating rate of $10^\circ\text{C min}^{-1}$ in the temperature range of 30 – 500°C . The UV-vis spectrophotometric measurements were done on an Agilent Technologies Cary 60 UV-vis spectrophotometer. The composition of the material was assessed by X-ray Photoelectron Spectroscopy (XPS) using PHI 5000 Versa Probe III spectrometer.

3.2.4. Measurements of Swelling Characteristics

The swelling value of hydrogel in deionized water was investigated using gravimetric method at room temperature. The capacity of hydrogel to retain water, its swelling characteristic under different pH and salt concentrations were also monitored. Protocol for determining the swelling characteristics have been discussed below:

3.2.4.1. Swelling Kinetics

100 mg air dried uniformed sized hydrogel was weighed and immersed in de-ionized water. Swollen gels were withdrawn from water and excess of solvent on surface was wiped off using tissue paper and weighed at predetermined time intervals. Weight determination was carried out upto the attainment of constant weight. Equilibrium Water Absorbency (EWA) was calculated using the formula:

$$WA = \frac{W_t - W_0}{W_0} \text{-----} (1)$$

Where, W_0 (mg) and W_t (mg) are the weight of dry and swollen hydrogel samples.

3.2.4.2. pH and Salt Sensitivity

100 mg of dried hydrogel sample was immersed in buffer solution of different pH (2-12) at room temperature for assessment of pH dependent EWA. The pH values of buffer solutions were adjusted using 1 mol L⁻¹ NaOH and 1 mol L⁻¹ HCl. The equilibrium water absorbency was calculated using equation (1) at each pH value. Different concentration of KCl solution (0.2, 0.6, 1.0 wt %) was used to determine water uptake ability of hydrogel in salt solution using the same method.

3.2.4.3. Water Retention Capacity

To study the water retention capacity of the hydrogel at equilibrium known amount of air dried hydrogel sample was kept in distilled water for one day. Swollen hydrogel was removed and weighed at regular time interval to investigate water retention capacity. The water retention ratio was calculated using the formula:

$$WR(\%) = \frac{(W_t - W_0)}{(W_e - W_0)} \times 100 \text{-----} (2)$$

where, W_0 is the weight of initial dried hydrogel, W_e is the weight of swollen hydrogel at equilibrium and W_t is the weight of swollen hydrogel at time 't'.

3.2.5. Adsorption of Dyes

Methylene Blue and Methyl Orange were selected as model cationic and anionic dyes respectively, and batch adsorption experiments were carried out to investigate the adsorption efficiency of hydrogel. The experiments were carried by varying different parameters like adsorbate concentration, hydrogel dosage, temperature and pH. The adsorption isotherm was also determined and kinetics for the phenomenon of adsorption was also determined.

Briefly, immersion of known amount of dried hydrogel in distilled water to attain equilibrium swelling state. The swollen hydrogel was then added into 50 mL of aqueous dye solutions of predetermined concentrations (50, 100, 150, 200 and 250 mg L⁻¹) under stirring at room temperature for 24 hours. To determine the optimum amount of hydrogel to be used for further experiments different quantities of hydrogel (25, 50, 100, 150, 200 mg) were added to 100 mg L⁻¹ of MB and MO solution respectively. For pH variation study 100 mg L⁻¹ of dye solutions with different pH values were prepared and 100 mg of hydrogel was added to determine the fate of adsorption. The pH adjustments were done using NaOH and HCl solutions.

Using the optimized conditions kinetics experiment was performed at different time intervals. The effect of temperature on adsorption was also determined by performing the experiments at 35 °C and 45°C. For quantification of adsorption, supernatants were collected by filtration after each set of adsorption experiment and measured using UV-Vis spectrophotometer (wavelength scan range: 200-800 nm) at $\lambda_{\max} = 664$ for MB and $\lambda_{\max} = 460$ for MO. The volume of supernatant removed is replenished by the same volume of fresh dye solution to maintain uniform concentration of dye throughout the experiments. Each experiment was conducted in triplicate and mean values have been reported. The adsorption capacity, removal percentage and adsorption at particular time 't' were calculated using the formula:

$$q_e = \frac{(C_0 - C_e)}{m} \times V \text{ ----- (3)}$$

$$\%R_e = \frac{C_0 - C_e}{C_e} \times 100 \text{ ----- (4)}$$

$$q_t = \frac{C_0 - C_t}{m} \times V \text{ ----- (5)}$$

where, q_e is the adsorption capacity (mg/g), % Re denote removal efficiency and q_t represents the adsorption capacity at particular time ' t ' (mg/g); C_0 is the initial concentration (mg L⁻¹), C_e is equilibrium concentrations (mg L⁻¹) and C_t denotes concentration at time ' t ' (mg L⁻¹) of dyes in aqueous solution; ' V ' represent the volume of dyes solution (L); and ' m ' denotes the weight of the hydrogel (g).

3.2.6. Desorption Experiment and Reusability

After completion of adsorption process, the dye loaded hydrogel was separated by filtration process and further washed using deionized water to remove un-adsorbed dye. In order to select the most appropriate solvent media for desorption the dye loaded hydrogel was immersed in 0.1 mol/L of HCl, 0.1 mol/L of NaOH and 0.1 mol/L of NaOH solutions and various solvents like methanol, acetone and ethanol were also screened. Saturated hydrogel was added to 20 mL of desorption media taken in an erlenmeyer flask kept under stirring upto the complete regeneration of hydrogel for 8 hours. The Hydrogel was then separated and washed with deionized water followed by acetone to remove excess of desorption media and then dried for reuse.

3.2.7. Preparation of Ag@Hydrogel

Ag loaded hydrogel was prepared by adding 10 mL AgNO₃ (0.5 M) to a solution of 20 mL alcohol containing 100 mg of swollen hydrogel in a stoppered Erlenmeyer flask. The resultant solution was sonicated for 10 minutes. 25% of hydrazine hydrate was used as reducing agent and added slowly dropwise at an interval of 5 minutes. The reaction kept under stirring in dark for 24 hours to ensure complete reduction of silver ions. The product was separated by filtration and washed with water and acetone. The dried sample was stored under vacuum.

3.2.8. Reduction of 4-NP Catalyzed by Ag@Hydrogel

The catalytic reduction of 4-NP was carried out in a quartz cuvette in the presence of Ag@Hydrogel and NaBH₄. To study the catalytic efficiency, 10 mg of catalyst was added to 4-NP solution of varying concentrations (10 mM, 25 mM, 50 mM and 100 mM). Sodium Borohydride (5.53 mM) was used as a reducing agent. The stock solutions of 4-NP and NaBH₄ were added to a quartz cuvette one after the other. At this stage, the *p*-Nitrophenol was converted to *p*-nitrophenolate anion. Then catalyst and DI water were added to keep the volume of the mixture to 2.0 mL. Similar reactions were carried out in the presence of sunlight light to study

the photocatalytic effect. The reaction was monitored using UV-vis spectrophotometer at different time intervals. The Ag@Hydrogel was recycled in 1:1 mixture of water and acetone. The catalyst could be recycled 5 times after the reduction reaction.

3.3. Results and Discussion

3.3.1. Characterization Techniques

3.3.1.1. Solid State NMR Spectra Analysis

The NMR spectrum in **Figure 3.2** shows expected peaks corresponding to both dextran molecule and urethane linkages. The carbon corresponding to dextran ring appears at $\delta = 94.30$ and 68.68 ppm. The peaks appearing at 26.71 , 35.99 and 39.25 ppm symbolizes methylene carbon. Anomeric carbon linkages appear at 122.91 ppm. The peaks corresponding to urethane linkages appear at 155.87 ppm suggesting the formation of crosslinked hydrogel ³⁵.

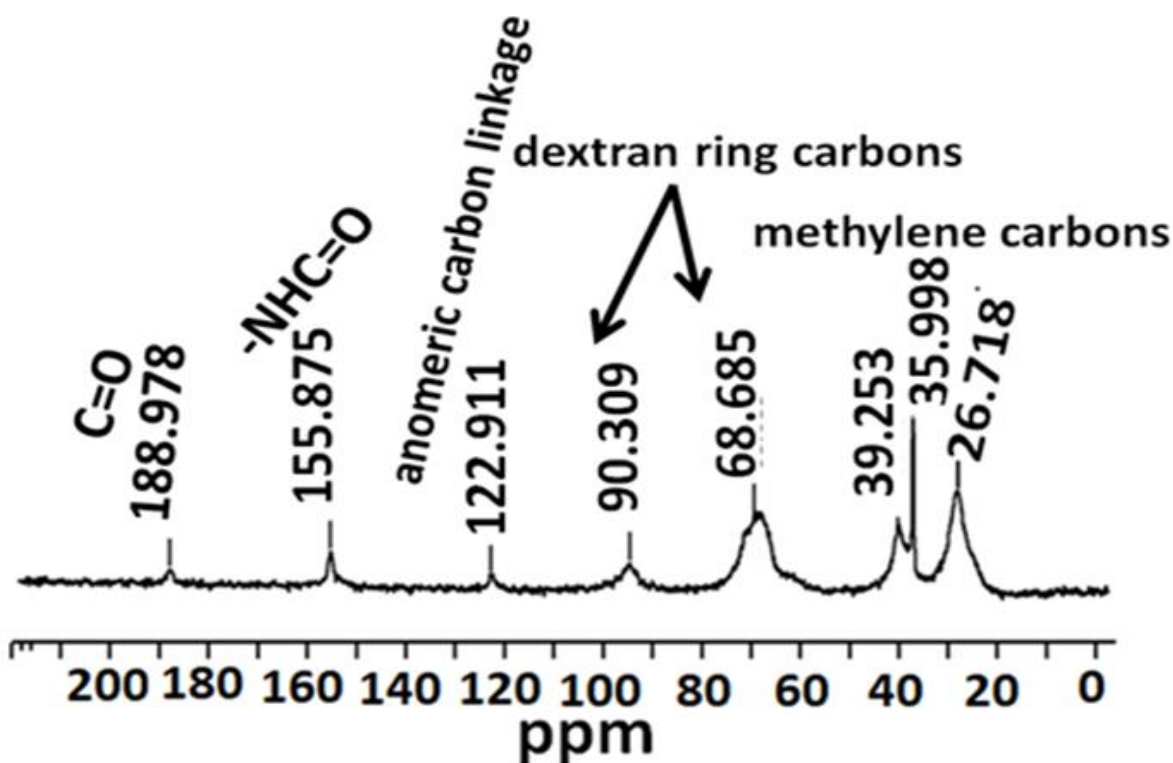


Figure 3.2: Solid state ^{13}C NMR of Hydrogel

3.3.1.2. FTIR Spectra Analysis

The FTIR spectrum of dextran shows characteristic peaks corresponding to O-H stretching vibration at 3321 cm^{-1} . The peaks corresponding α -1,6-glycosidic bond of dextran appear at 1023 cm^{-1} . Further, the presence of peak at 1015 cm^{-1} arises due to chain flexibility of dextran around α -1,6-glycosidic bonds³⁶. The bands at 835 cm^{-1} and 762 cm^{-1} represent presence of alpha anomeric carbon and pyran ring³⁷. The spectrum of the hydrogel shows the presence of all the peaks corresponding to dextran and additional peaks for C=O and NH groups corresponding to urethane linkages are observed at 1567 and 2929 cm^{-1} respectively as shown in **Figure 3.3**. Thus, the structure of hydrogel was confirmed.

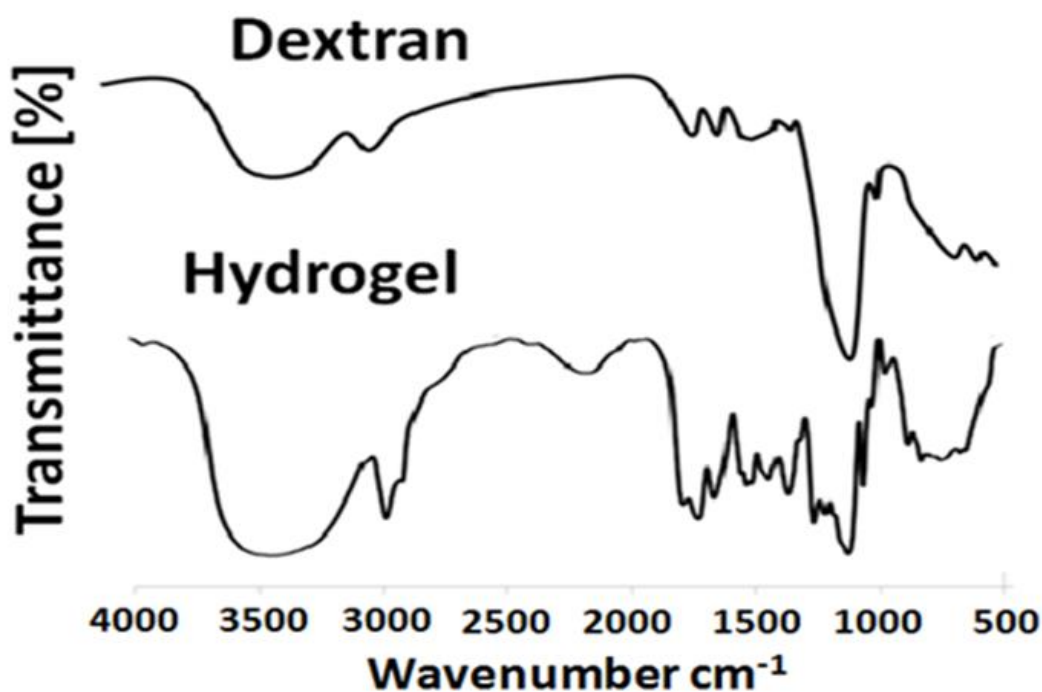


Figure 3.3: FTIR spectra of Dextran and Hydrogel

3.3.1.3. XRD Analysis

The comparison of the X-ray diffraction patterns (**Figure 3.4**) of pure dextran and Dextran modified with HMDI shows distinct changes suggesting the polymerization. Five distinct peaks corresponding to characteristic A-type X-ray diffraction pattern representing the crystalline nature of dextran were observed at 2θ values of 15° , 17° , 18° , 21° , and 29° in the spectrum³⁶. Upon polymerization with HMDI the sharp peaks are replaced by broad weak peaks which

suggest the replacement of the hydroxyl group of dextran molecules by other functionalities. Crystallinity is observed in dextran due to the formation of intermolecular and intramolecular hydrogen bonds³⁸. These bonds are readily weakened by the introduction of other functional groups and the ordered crystalline structure is distorted due to decrease in the number of hydroxyl groups³⁷. Thus the diffraction pattern of HMDI modified dextran shows amorphous nature.

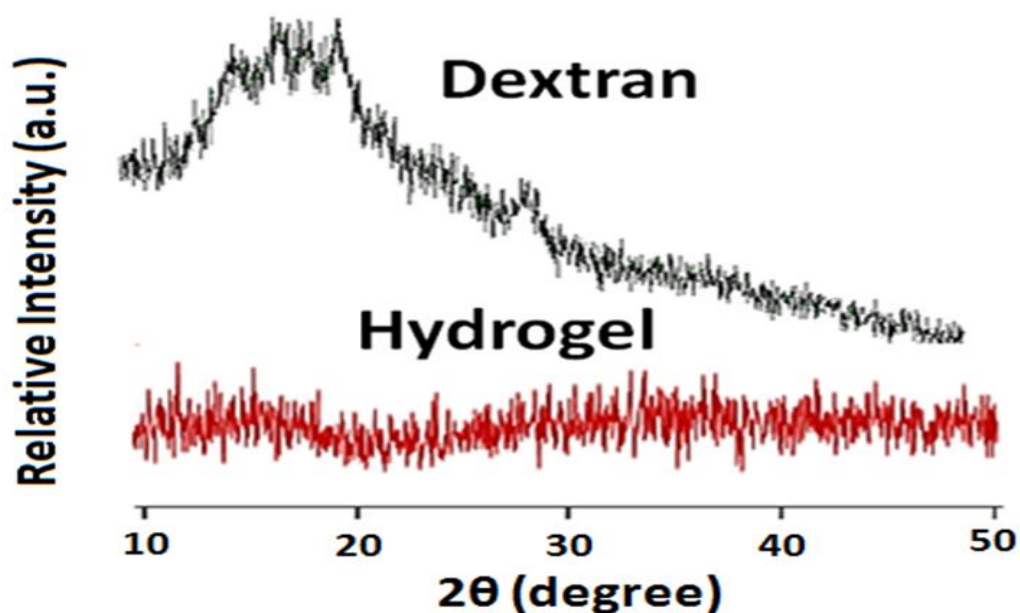


Figure 3.4: X-ray diffractograms of Dextran and hydrogel

3.3.1.4. EDS Analysis

The elemental composition of the hydrogel as a representative of the bulk sample shows the presence of elements like C, N and O represented in **Figure 3.5**. The detection of N in hydrogel sample which is absent in dextran sample indicates the successful formation of urethane linkages.

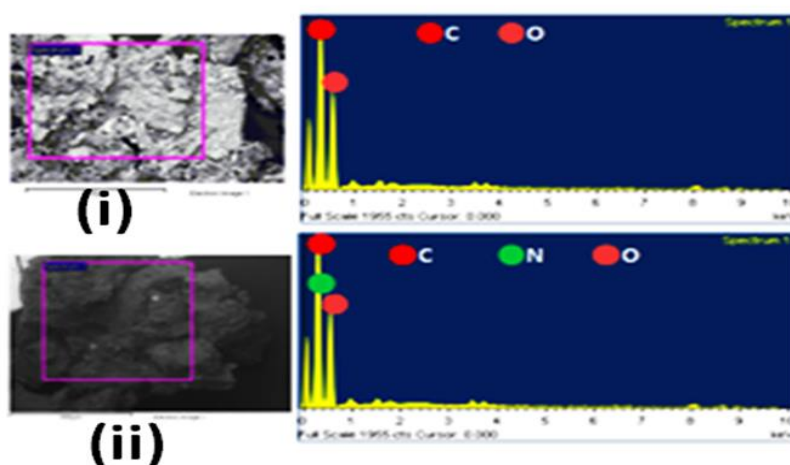


Figure 3.5: SEM images and elemental mapping via EDX in (i) dextran and (ii) hydrogel

3.3.1.5. Thermogravimetric Analysis

The mass loss was observed in three stages. The loss of 10% in the range of 30 °C to 150 °C corresponds to the removal of traces of moisture from the polymer³⁷. The second stage degradation occurs in a temperature range of 160-350 °C with a significant weight loss of 55 % due to breakdown of urethane linkages. The mass loss of 17 % after 360 °C is due to degradation of organic matter of dextran as shown in **Figure 3.6**³⁹.

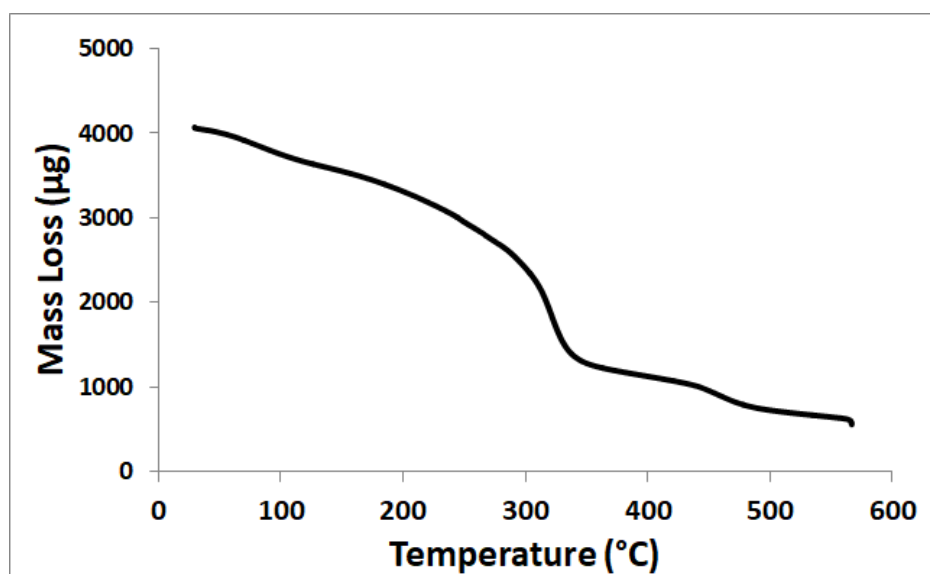


Figure 3. 6: Thermogravimetric Curves for Hydrogel

3.3.2. Swelling behavior of the hydrogel

The water uptake and retention capability of the synthesized hydrogel was assessed in deionized water. The swelling behavior at different pH values and the effect of salt was also assessed. These parameters were comprehensively analyzed for the assessment of practical applicability of the hydrogel.

3.3.2.1. Deionized water

The swelling behavior of hydrogel in de-ionized water is represented in **Figure 3.7 (A)**. The swelling ratio increases rapidly in initial stage between 0-200minutes, after 200 minutes the capability to encapsulate in coming water molecule decreases due to attainment of equilibrium. The presence of multiple hydroxyl functionalities in the dextran chain promotes the entry of water molecules in the hydrogel matrix immediately upon soaking which is observed in the initial stage of the study⁴⁰.

3.3.2.2. Different pH values

Hydrogel exhibited pH dependent swelling behavior with the equilibrium water absorbency increasing slowly with the increase in pH values (**Figure 3.7 (B)**). Low swelling was observed under acidic conditions (pH 2 to 6) and escalates under basic conditions (pH 8 to 12). This phenomenon is attributed to the dominance of hydrophobic interactions in the polymer chains under acidic conditions triggering the polymer to attain a collapsed state⁴¹. A collapsed polymer network restricts the traversing of water molecules which is evident from low swelling observed. Conversely, under basic conditions the hydroxyl group bearing a negative charge binds to the hydrophobic polymer chain and causes the polymer to expand and hence increase in swelling is observed⁴². Thus the conformational changes that occur in the polymer chains cause a pH swelling to occur.

3.3.2.3. Different concentration of saline solutions

Swelling ratio of the hydrogel was assessed in KCl solution of different concentrations was shown in **Figure 3.7 (C)**. It was observed that equilibrium swelling values significantly decreases from 74 g g⁻¹ to merely 27.7 g g⁻¹ upon increase in salt concentration. This can be ascribed to the difference in the osmotic pressure in the swelling solution and the solution within the polymeric matrix upon enhancement of salt concentration. The water molecules are expelled out due to this pressure difference causing the polymer to shrink at higher concentrations⁴³.

3.3.3. Water retention profile of the hydrogel

Figure 3.7 (D) represents water retention capacity of the hydrogel. The graph shows a swift decrease in water retention (50 %) at preliminary stage of heating (<100 minutes) that becomes sluggish after 200 minutes. The dehydration of polymer chains that is a driving force of deswelling causes a decrement in it. Further, multiple hydroxyl groups bearing dextran has an affinity for water and hence it turns in to a water emancipating channels aiding the deswelling and hence the shrinking of polymer chains⁴⁴.

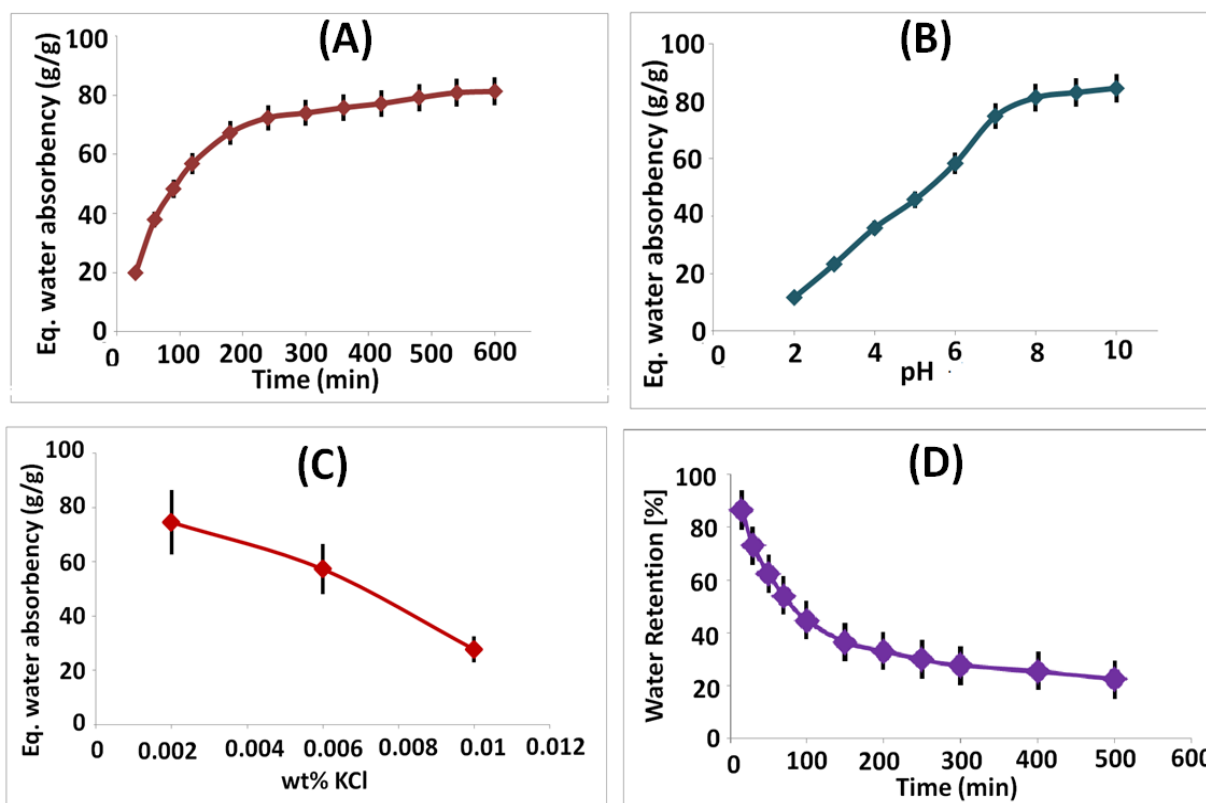


Figure 3.7: Swelling characteristics of hydrogel in (A) distilled water (B) buffer solutions of pH (2-10) (C) KCl solutions (D) water retention profile

3.3.4. Effect of various parameters on adsorption of dyes

3.3.4.1. Effect of pH

The pH of the dye solution plays significant role in determining its removal efficiency as it affects the extent to which it can ionize. Further a change in pH also influences the surface charges on adsorbent. Both the above mentioned factors contribute towards dye molecules

adsorption on hydrogel surface. In case of MB adsorption as per **Figure 3.8 (A)** a change in pH of the solution from 2-12 causes a drastic increase in removal efficiency from 40% to 94%. This is attributed to hydroxyl groups which exists as ionized O⁻ form and has an increased affinity towards cationic MB. In case of MO the maximum adsorption of 77% was observed under acidic conditions. Electrostatic interactions and hydrogen bonding exist between hydrogel and dyes. These are the main factors responsible for showing difference in the adsorption behavior of MB and MO³⁴.

3.3.4.2. Effect of the Hydrogel Dosage

The amount of hydrogel is an important parameter to optimize adsorption mechanism in dye removal as it is directly concerned with available active sites. The presence of many active sites and functional groups can be adequately employed at higher dosage of adsorbent which leads to higher adsorption capacity⁴⁵. The same phenomenon is observed in this case as the removal efficiency of dyes increases with increase in hydrogel dose as shown in **Figure 3.8 (B)**.

3.3.4.3. Effect of Initial Concentration

The effect of the initial concentration on equilibrium adsorption capacity is represented in **Figure 3.8 (C)**. The adsorption efficiency increases upon an increase in the initial concentration upto 150 mg/L. As the concentration reaches 200 mg/L the removal of dye becomes sluggish²¹. In case of MB the decrease is from 94% to 53%, whereas for MO the reduction is from 72% to 42%. The rapid dye intake is because of an enhanced mass gradient arising between adsorbent and adsorbate as a result of high initial concentration. This acts as driving force for the transfer of dye molecules from solution to hydrogel surface. Later, the decrease in removal efficiency on increasing the concentration is due to repulsion between dye molecules in the solution and those on hydrogel surface. The decrease in the availability of free functional sites for adsorption can be cited as another reason for this decrease⁴⁶.

3.3.4.4. Effect of Temperature

Higher temperature is favorable for adsorption of dyes. An increase in temperature by 10 °C causes a 4% increase in the removal efficiency. This is shown in **Figure 3.8 (D)** where the %Re of MB increases from 91% to 95% to 98% and for MO the increase is from 75% to 80% to ~85% while increasing the temperature from 35°C to 45°C to 55°C respectively. Increasing the

temperature provides required energy by enhancing the motility of dye molecules and for establishment of interactions between adsorbent and adsorbate molecules⁴⁵.

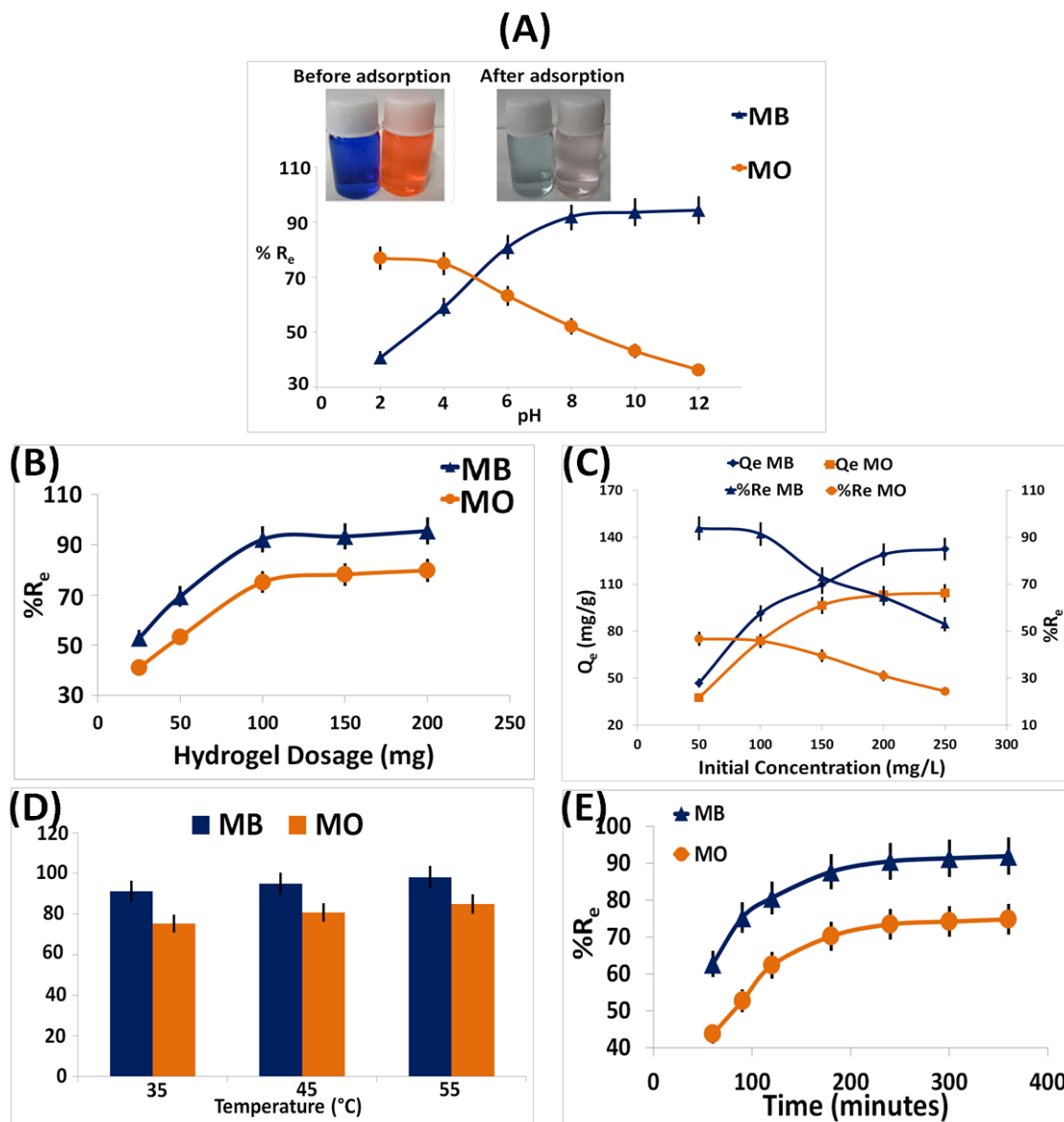


Figure 3.8: Effect on removal efficiency of MB and MO by varying parameters (A) pH; Inset: Photographs of vial before and after adsorption, pH 12 for MB and pH 2 for MO (B) adsorbent dosage (C) initial concentration (D) at 35°C, 45°C and 55°C temperature (E) contact time (For all the experiments 100 mgL⁻¹ dye solution was used and 0.1 g of hydrogel was used)

3.3.4.5. Effect of Contact Time

Effect of contact time on adsorption of dyes by hydrogel at 60, 90, 120, 180, 240, 300 and 360 minutes (at pH 12 for MB and pH 4 for MO) was shown in **Figure 3.8 (E)**. Equilibrium time for adsorption of dyes was attained at 360 minutes. The removal efficiency for both dyes is different when equilibrium is attained because of their interactions with hydrogel. The removal of MB is faster than MO. The disappearance in color of the dye solutions and the appearance of the color on the hydrogel surface over a period of time is an indication of adsorption occurring. The rapid adsorption upon initial exposure is a result of available free functional groups the later decrease in adsorption on increased time of contact is because of surface saturation and repulsive forces acting on the surface. An attainment of balance between the driving force causing adsorption and repulsive forces leads to equilibrium state and hence no further adsorption⁴⁷.

3.3.5. Adsorption Isotherm

Adsorption isotherms are generally used to explain the interaction between adsorbate and adsorbent as well as optimum use of adsorbent in solution. Broadly, two isotherm models used to describe adsorbate-adsorbent interactions are Langmuir and Freundlich isotherm models.

$$\frac{C_e}{q_e} = \frac{1}{K_L} + \frac{C_e}{q_m} \text{----- (6)}$$

$$\ln q_e = \ln K_F + \frac{1}{n} \ln C_e \text{----- (7)}$$

where, C_e (mg L^{-1}), q_e (mg g^{-1}), q_m (mg g^{-1}), K_L (L/mg) and K_F (L/mg) represents the equilibrium concentration of dyes, the adsorption capacity of SPNAs at equilibrium, the maximum adsorption capacity, Langmuir and Freundlich equilibrium adsorption constants respectively. The value of K_L is an indication of favorable ($0 < K_L < 1$), unfavorable ($K_L > 1$) or linear ($K_L = 1$) adsorption process⁴⁸.

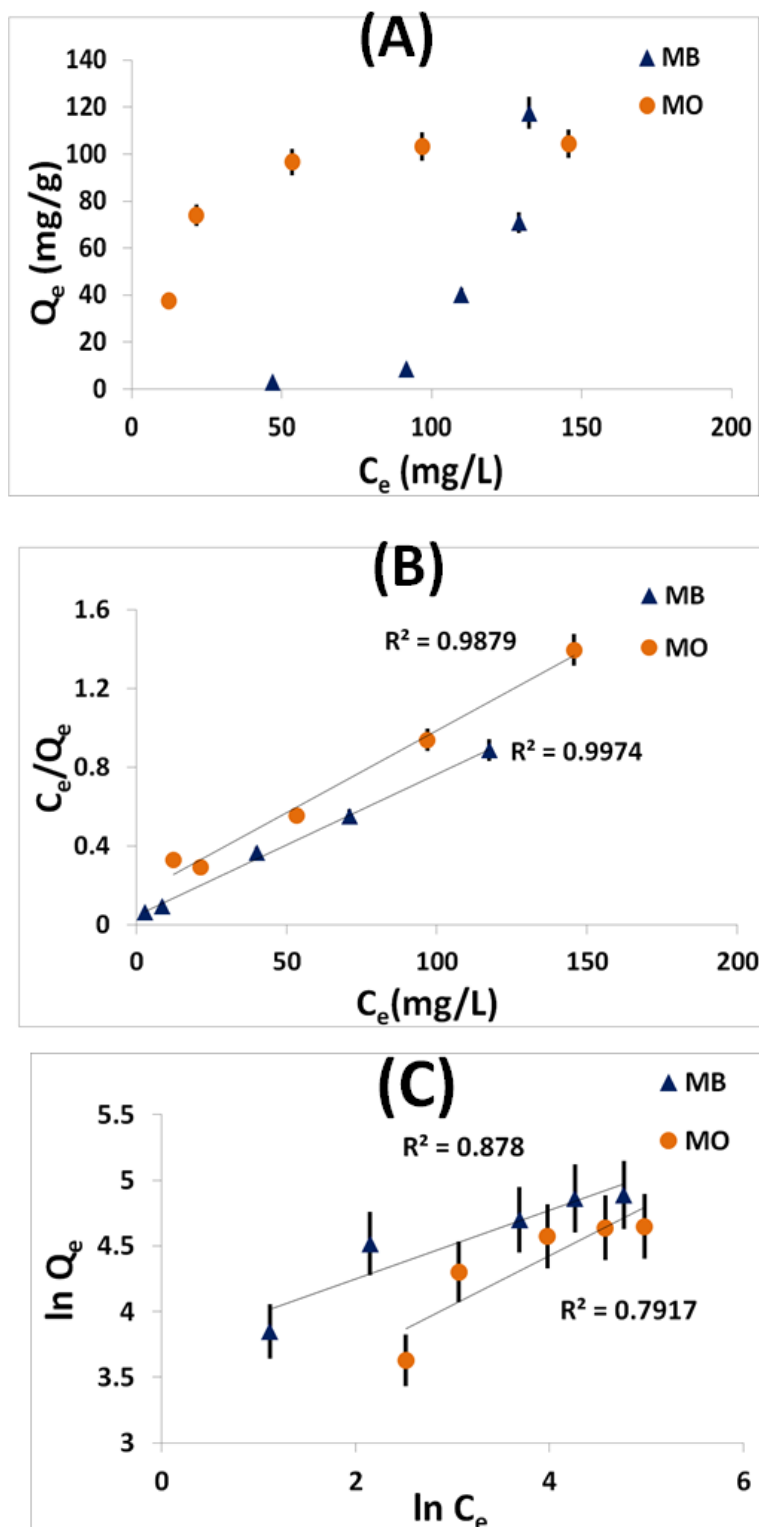


Figure 3.9: Adsorption isotherms for MB and MO uptake; (A & B) Langmuir and (C) Freundlich model fitting

The experimental data was fitted to both the isotherm models (**Figure 3.9**) and the values of correlation coefficient suggest that the adsorption of dyes fits better in the Langmuir isotherm model leading to a monolayer adsorption⁴⁹. The value of $0 < K_L < 1$ (**Table 3.1**) indicates that process of adsorption is favorable for both the dyes.

Table 3.1: Isotherm Constants for the Adsorption of 100mgL⁻¹ of Methylene Blue and 100 mgL⁻¹ of Methyl Orange

Dye Molecule	Langmuir			Freundlich		
	q _m (mg g ⁻¹)	K _L (L mg ⁻¹)	R ²	N	K _F (L g ⁻¹)	R ²
Methylene Blue	142.857	0.0557	0.997	3.831	1235.21	0.878
Methyl Orange	125	0.0302	0.987	2.673	21.01	0.791

3.3.6. Adsorption Thermodynamics

Adsorption thermodynamics were calculated for the dyes to assess the spontaneity of its removal. Various parameters like Gibbs free energy (ΔG°), Free energy change (ΔH°), and change in entropy (ΔS°), were calculated from thermodynamic equilibrium constant (K_c) using appropriate equations as mentioned below:

$$K_c = \frac{a_s}{a_e} = \frac{v_s q_e}{v_e C_e} \text{-----} (8)$$

Here a_s stands for the activity of the dye molecules ions adsorbed on the surface of hydrogel and a_e its activity within solution at equilibrium; v_s and v_e are the activity coefficients of the dye molecules while they are adsorbed and in solution at equilibrium, respectively.

It is known that when concentration of adsorbate decreases and approaches zero, the activity coefficient v approaches closer to unity, under such circumstances and hence equation 8 can be represented as:

$$\lim_{C_e \rightarrow 0} \frac{a_s}{a_e} = \frac{q_e}{C_e} = K_c \text{-----} (9)$$

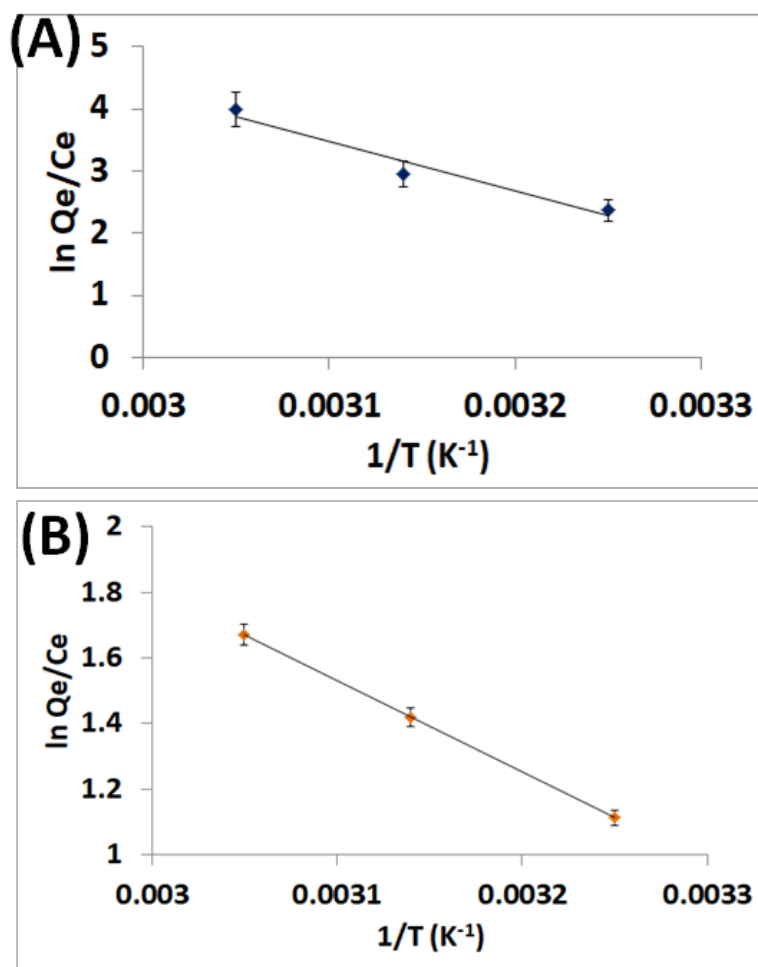


Figure 3.10: Thermodynamic plot for removal of (A) MB and (B) MO using hydrogel

The values of K_c have been calculated from the plot of experimental data of $\ln q_e/C_e$ versus q_e at three different temperature 308, 318 and 328 K. Then Gibbs free energy has been calculated as per the equation 10.

$$\Delta G^\circ = -RT \ln(K_c) \text{ ----- (10)}$$

Further free energy and entropy calculations have been done as per Van't Hoff plot of $\ln K_c$ versus $1/T$ (**Figure 3.10**) and thermodynamic surface plot has been shown in **Figure 3.11**.

$$\ln K_c = \frac{\Delta S^\circ}{R} - \frac{\Delta H^\circ}{R} \cdot \frac{1}{T} \text{ ----- (11)}$$

The studies show an increase in the ΔG° value with increasing temperature as shown in **Table 3.2**. Moreover, its negative value suggests the removal of dyes is a spontaneous process favored by increase in temperature. The positive value of ΔH° reveals the adsorption assisted by hydrogel is endothermic in nature. It is also reported that value of ΔH° in the range $2.1\text{--}20.9\text{ kJ mol}^{-1}$ results in interactions which are physical giving rise to (physisorption) and values lying between $80\text{--}200\text{ kJ mol}^{-1}$ represent chemisorption. Since the calculated values are greater than 20.9 , the process of dye removal via synthesized hydrogel follows chemisorption. This corroborates with the kinetics modelling obtained.⁵⁰

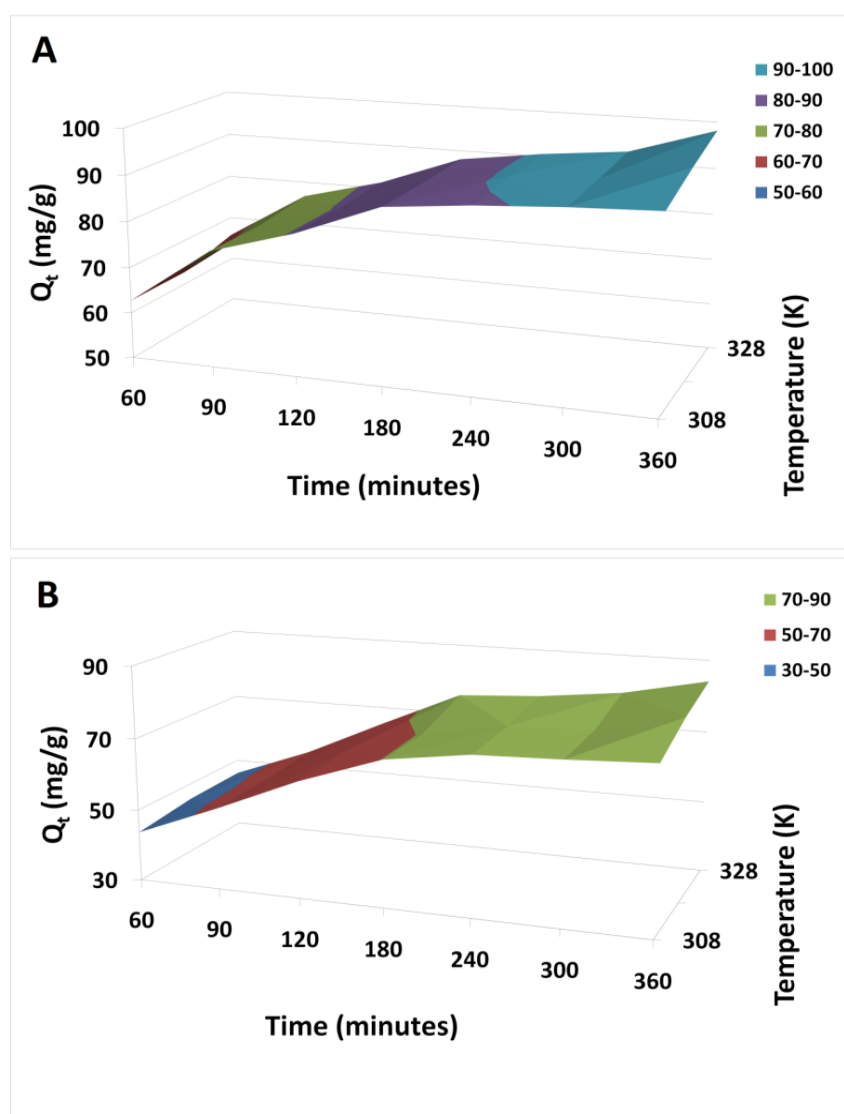


Figure 3.11: Thermodynamic surface plots for (A) MB and (B) MO uptake by hydrogel

Table 3.2: Thermodynamic Parameters for adsorption of dyes onto the surface of hydrogel at three different temperatures

Dyes	K _c			ΔH° (kJ/mol)	ΔS° (kJ/mol. K)	ΔG° (kJ/mol)		
	308 K	318 K	328 K			308 K	318 K	328 K
MB	2.36	2.95	3.99	66.6	0.23	-6.06	-7.82	-10.9
MO	1.11	1.41	1.67	23.2	0.08	-2.85	-3.75	-4.56

The positive ΔS° value is an implication of an increase in the randomness at the interface of dye solution and adsorbent surface as adsorption process occurs. This represents an affinity of the dye molecules towards adsorbent as a result of an increase in the degree of freedom.⁵¹

3.3.7. Adsorption Kinetics

The determination the kinetics of dye adsorption gives crucial information regarding the mechanism involved in the process of adsorption. Various models (zero order, first order, second order, third order, pseudo first order, and pseudo second order) were employed as expressed in the following equations to ascertain the kinetics of dye removal using hydrogel.

$$\ln(q_e - q_t) = \ln q_e - k_1 t \text{----- (12)}$$

$$\frac{t}{q_t} = \frac{1}{k_2 q_e^2} + \frac{t}{q_e} \text{----- (13)}$$

Here, q_e is the amount of adsorbed dye at equilibrium and q_t (mg g⁻¹) is the amount of adsorbed dye at time t (minutes). The pseudo-first order and pseudo-second-order rate constants are expressed as k_1 and k_2 (mg min g⁻¹) respectively. The experimental data fits well in the pseudo second order model with correlation coefficient of 0.987 for MB and 0.976 for MO as represented in **Figure 3.12**. This leads to a conclusion that the adsorption of dye molecules is influenced by its chemical interactions with hydrogel suggesting that chemisorption is rate determining step⁴⁵.

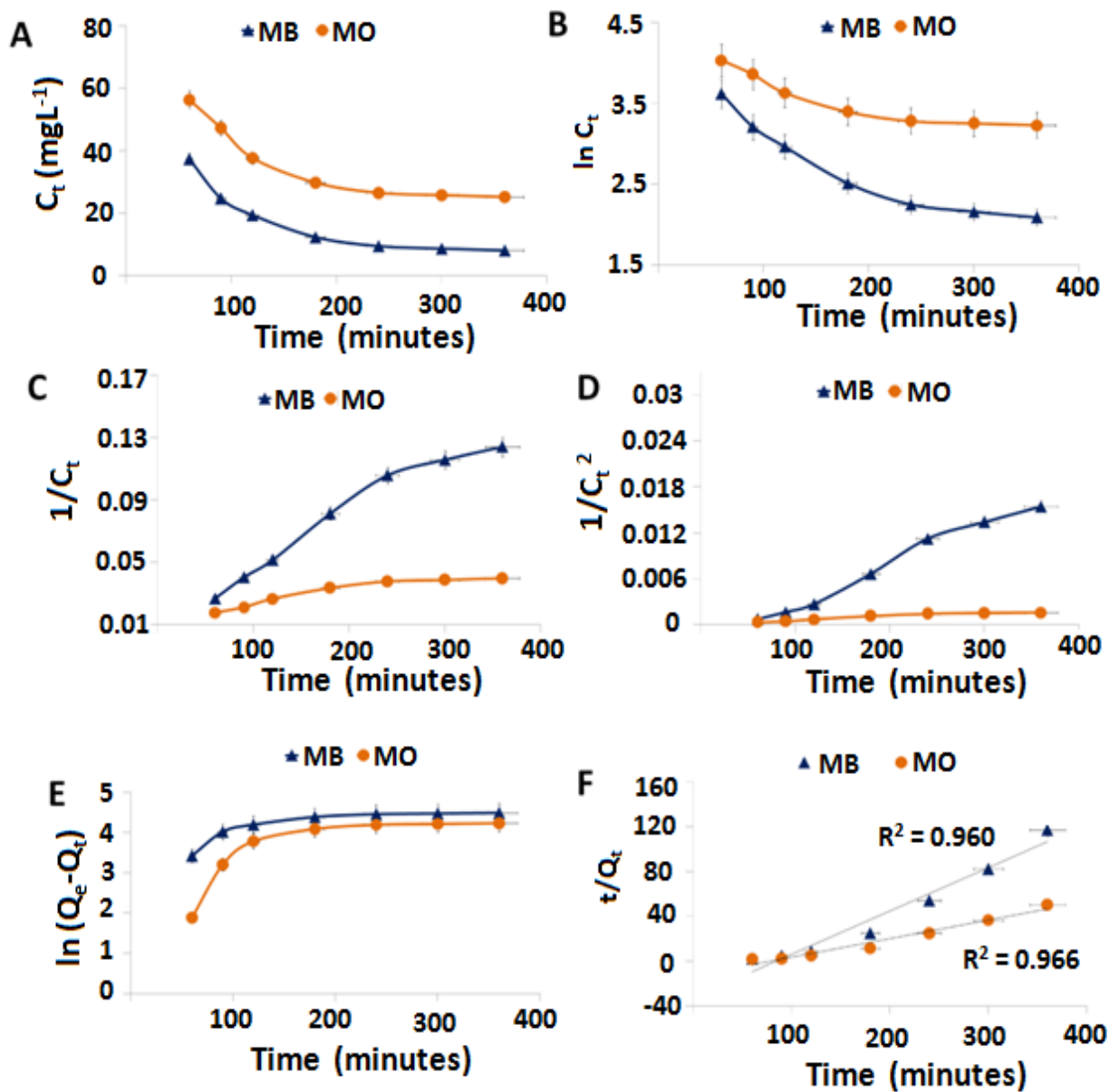


Figure 3.12: Graphs of (A) zero order (B) first order (C) second order (D) third order (E) pseudo first order (F) pseudo second order kinetic models for adsorption of MB and MO on hydrogel (conditions: initial concentration 100 mgL⁻¹, adsorbent dosage 0.1g at room temperature)

3.3.8. Adsorption Studies in Binary Mixture of Dyes

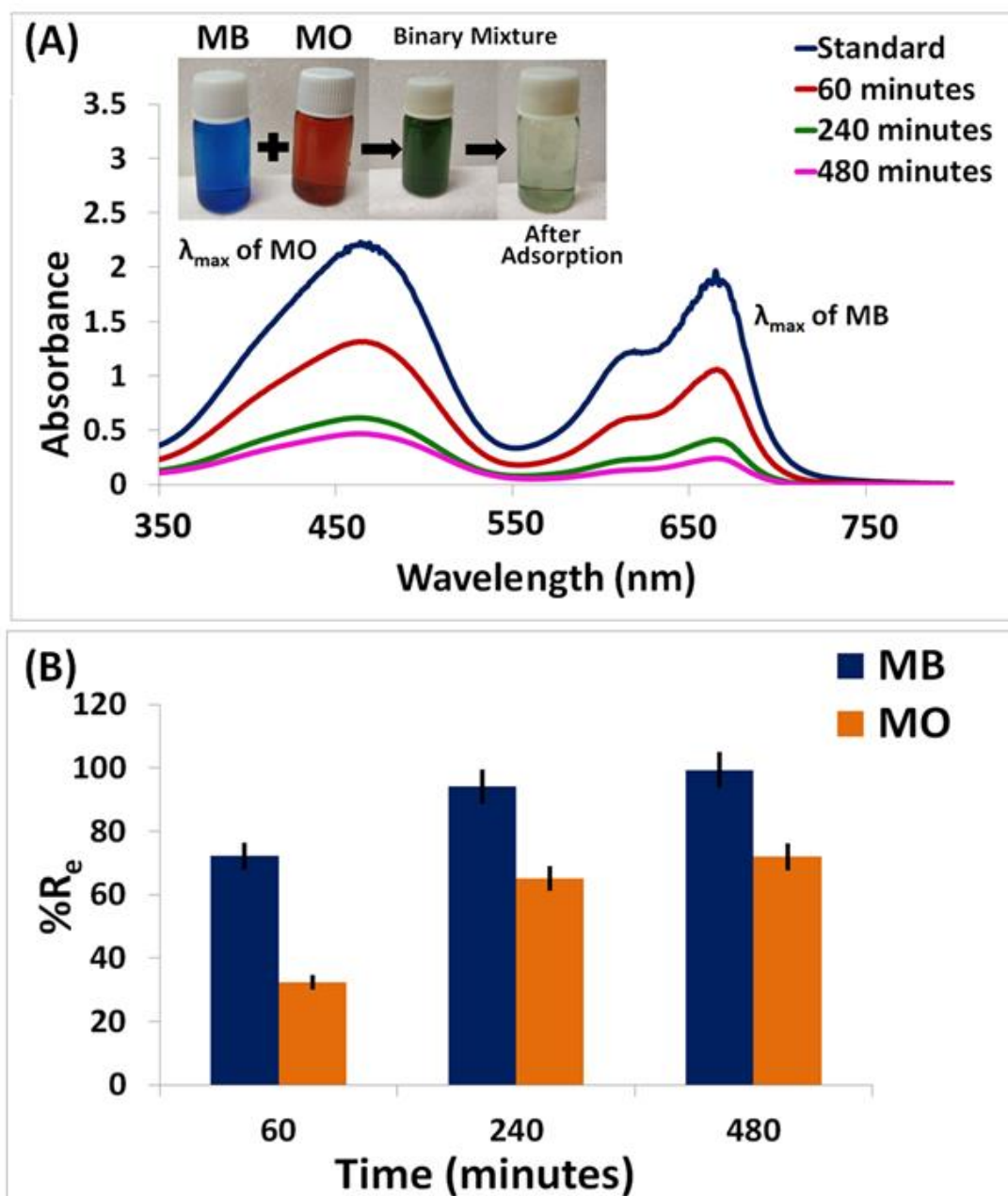


Figure 3.13: Assessment of hydrogel's adsorption behaviour in a binary mixture of dyes (A) UV-vis spectra recorded before and after adsorption at different time intervals digital (Inset: images depicting color changes prior to mixing, after mixing of dyes and post adsorption.) (B) % R_e for MB and MO individually from mixture (Conditions: initial concentration of binary solution 25 mgL^{-1} , adsorbent dosage 0.1 g at room temperature)

The study of adsorption in a binary mixture of MO and MB was carried out by adding 10mL of 50 mg/L MB and 10mL of 50 mg/L MO to obtain 20 mL solution of 25 mg/L for both MB and MO. Adsorption in a binary mixture of MO and MB shows a greater removal of MB (99%) as compared to MO (76%). The residual color in the treated water is due to presence of traces of unadsorbed MO (Figure 7A and the inset photograph). The adsorption of both the dyes simultaneously in presence of the hydrogel was determined with the help of adsorption capacities (Rq) as shown in equation 14.

$$Rq = \frac{qb,i}{qm,i} \text{-----}(14)$$

where, qb,i and qm,i are the quantities of dye uptake i in the binary system and monocomponent system with the same initial concentrations, respectively. The removal efficiency of MB was observed to be 99.3% and for MO is 75.9% indicating efficient adsorption performance of hydrogel even in mixtures (**Figure 3.13**).

In the case of simultaneous there can be three possibilities one can be the case of synergism when (i) if $Rq > 1$ in this the adsorption of one dye is increased due to the presence of other dyes; case 2 can be of antagonism when (ii) if $Rq < 1$ the adsorption of one dye suppresses the removal of other dye and of non-interaction (iii) if $Rq = 1$, wherein adsorption of each dye is independent of the presence of other dye. In this case, we discovered that the value of Rq of greater than 1, which suggests that, it is a case of synergism. Thus hydrogel synergistically assists the removal of both the dyes. There is no reciprocated antagonistic effect on the phenomenon of adsorption when they co-exist in a mixture⁵². The reason for this behavior is the prevalence of two different dominating interactions responsible for the adsorption of both the dyes.

3.3.9. Desorption and Recyclability

The possibility of regeneration and reuse are important indices for the practical applicability and cost effectiveness of adsorbents⁵³. Successive adsorption/desorption cycles were performed to investigate reusability and stability of hydrogel. For desorption experiments 0.1 mol L⁻¹ HCl, NaOH and NaCl solutions have been used. As per **Figure 3.14 (A)** the recycling efficiency for MB was 92%, 74% and 0% in HCl, NaOH and NaCl respectively. The regeneration efficiency for MO in HCl, NaOH and NaCl was 94%, 69% and 42% respectively. This concludes that 0.1

mol L⁻¹ HCl is the most suitable medium for the regeneration of hydrogel. As per **Figure 3.14 (B)** the adsorption capacity of the hydrogel decreases slowly after every cycle.

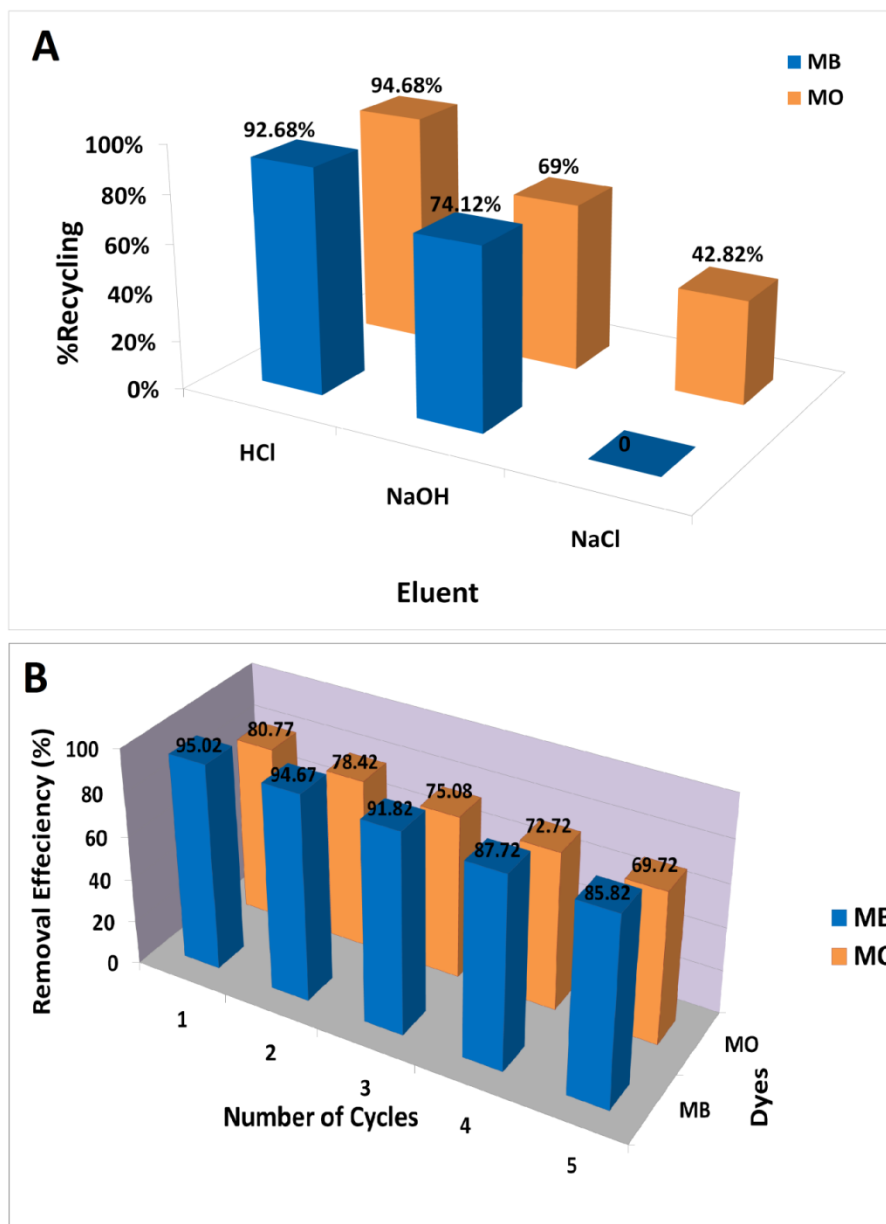


Figure 3.14: (A) Studies for desorption of dyes in different eluents (B) assessment of recyclability of the hydrogel

The regenerated hydrogel was characterized with XRD and IR (**Figure 3.15 (A)**) the results demonstrate no change in the characteristic spectra and diffractogram⁴⁵. This suggests that the hydrogel retains its structure and can efficiently remove the dyes. However, the increase in crystallinity observed in the diffractogram for dye loaded hydrogel is due to the adherence of dye

molecules in the polymer matrix. The enhanced crystallinity in MB loaded hydrogel as compared to MO loaded hydrogel proves more MB is adsorbed³⁸.

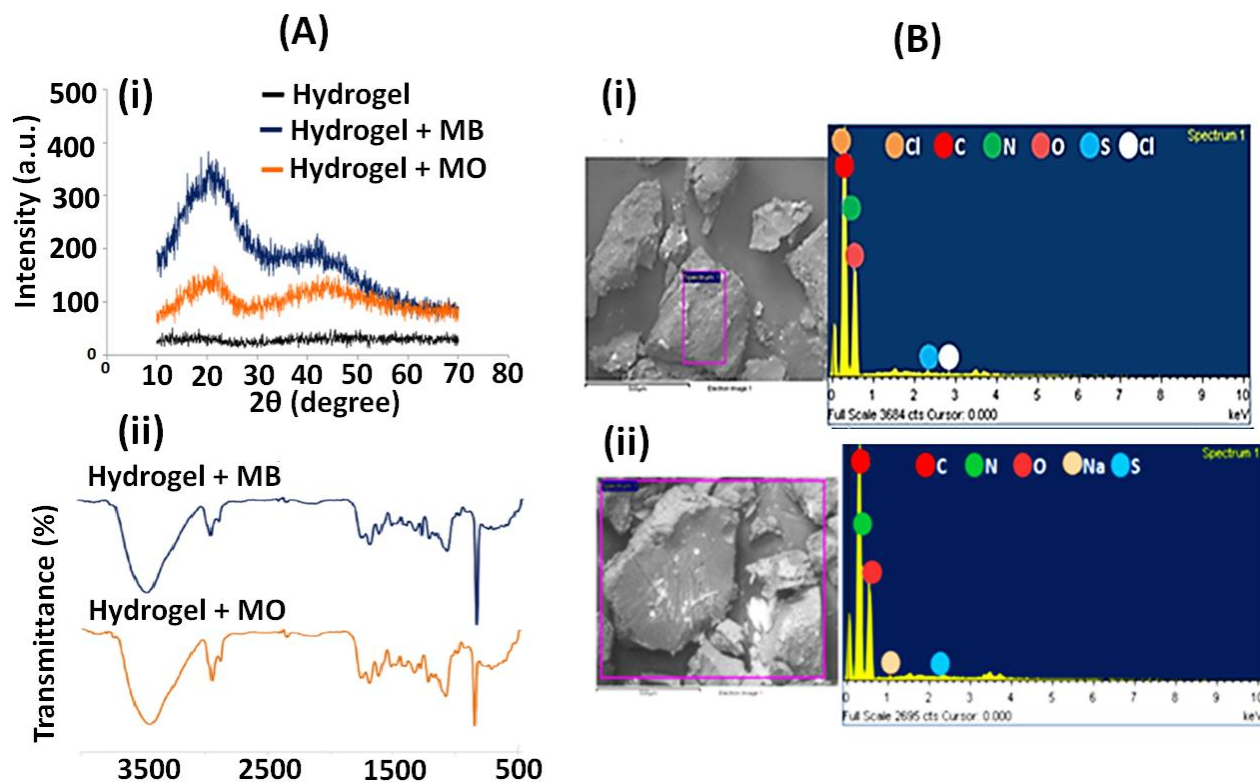


Figure 3.15: Characterizations of recycled hydrogel (A) (i) X-ray diffractograms and (ii) FTIR spectra (B) EDX spectra of adsorbent samples with dyes adsorbed on its surface (i) MB and (ii) MO

3.3.10. Adsorption Mechanism

The adsorption mechanism, in general, can be governed by various interactions like electrostatic forces of interactions, ion-exchange, hydrogen bonding, hydrophobic interactions and van der Waals forces. Of all these interactions, the forces actually being involved in adsorption will depend upon structural properties and functional groups of substrates and dye molecules^{54,34}. The planarity of dye molecules leads to formation of van der Waals forces between the dye molecules and hydrogel. The presence of surface functionalities leads to hydrogen bond formation⁴⁵. The probable interaction of cationic and anionic dye with hydrogel occurs *via* these interactions^{23,55}. This adsorption mechanism is further supported by effect of pH on MO and

MB adsorption on hydrogel ⁴⁵. The presence of elements corresponding to dye molecules appearing in the EDS spectra (**Figure 3.15 (B), Table 3.3**) after adsorption exhibits transfer of adsorbate molecules from dye solutions onto hydrogel is shown in **Figure 3.16**.

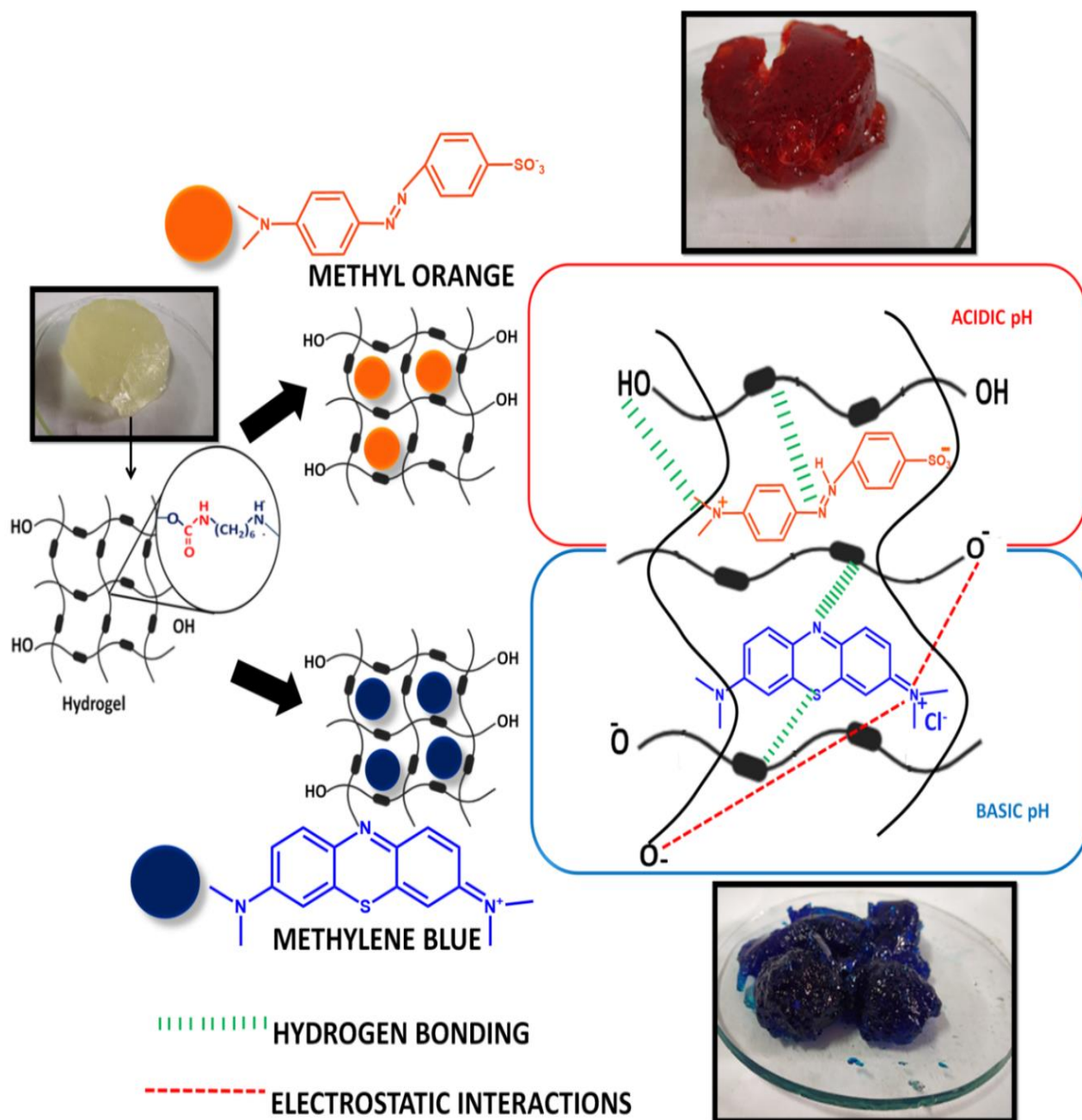


Figure 3.16: Probable mechanism for adsorption of cationic and anionic Dyes onto hydrogel depicting some possible interactions

Table 3.3: Elemental Composition of Recycled Hydrogel following Adsorption/Desorption Cycle

Material	C (wt-%)	N (wt-%)	O (wt-%)	Na (wt-%)	S (wt-%)	Cl (wt-%)
Hydrogel +MB	51.90	2.74	45.23	0	0.11	0.02
Hydrogel +MO	54.83	0.67	44.26	0.10	0.14	0

Adsorption of MB is facilitated due to the existence of hydroxyl groups and carbonyl functionalities in the polymeric matrix of hydrogel which created electrostatic force of interaction between hydrogel and cationic functionality of MB molecules. Whereas in case of MO the presence of sulfonate group decreases the scope of formation of attractive interactions, which is evident from the experimental data wherein less adsorption of MO has been observed as compared to MB. Further there is a possibility of formation of hydrogen bond between the amide and carbonyl groups of the polymer and amine functionalities on certain distinct changes are observed in the FTIR spectra and X-ray diffractogram before and after adsorption. There is an enhancement in the intensities of the peaks after dye adsorption which is attributed to presence of dyes on surface of hydrogel³⁸.

3.3.11. Comparison Table of other Hydrogels

Most of the adsorbents reported target removal of single dye as shown in **Table 3.4**. Those which demonstrate the removal of multiple dyes are composed of expensive materials. The waste management strategy for adsorbents or their value addition has also not been discussed.

Table 3.4: Comparison of Removal Efficiencies of Hydrogel with Literature Reports

Sr. No.	Adsorbent	Dye	Concentration	Q _e	Reference
1	DexG (Amphiphilic Cationic Dextran hydrogel)	Methyl Orange	1.5 mM	650-730 mg/g	⁵⁶
2	Alg/PASAP (alginate/polyaspartate hydrogel beads)	Malachite Green, Methylene Blue, Methyl	10 mg/L	600-700 mg/g MB, 300-350 mg/g MG	²³

		Orange			
3	Poly (N-isopropylacrylamide/ Acrylic Acid/N-allylisatin) hydrogel nanoparticles	Methylene Blue (300mg L ⁻¹), AuramineO(200 mg L ⁻¹), Chrysoidine G (150mg L ⁻¹)	250 mg/L	584 mg/g	57
4	poly(acrylic acid) (PAA)-based super-adsorbent nanocomposite Hydrogel	Methylene Blue	100 mg/L	2000 mg/g	34
5	Salecan/PAD hydrogels	Methyl Orange	10 mg/L	56.2 mg/g	21
6	Supramolecular Complex of Graphene Oxide and Sulfonatocalix[4]areneH hydrogel	Methyl Orange	20mg/L		3
7	Graphene/Chitosan based Hydrogel	Congo Red (CR)	100 mg/L	356 mg/g	58
8	GO-hydrogel porous nanocomposites	Methylene Blue	100 mg/L	714.29 mg/g	59
9	graphene oxide/sodium alginate/ polyacrylamide nanocomposite hydrogel	Methylene Blue Methyl Orange		2.62 mg/g, 1.24 mg/g	60
10	Sodium alginate poly itaconic acid (NaAlg/IA) hydrogel	Methylene Blue	80 mg/L	12.77 mg/g	61
11	β – Cyclodextrin-Cellulose / Hemicellulose-Based Hydrogels	Nickel, Cadmium	100 mg/L	18.6 mg/g 42 mg/g	62
12	Magnetic bentonite/ carboxymethyl chitosan/sodium alginate hydrogel beads	Copper	50 mg/L	56 mg/g	63
13	Dextran Hydrogel	Methylene Blue, Methyl Orange	100mg/L	98 mg/g 84 mg/g	This Work

3.3.12. Valorization of Waste Expensive Metal Ions entrapped in the hydrogel matrix to Valuable Metal Nanoparticles for removal of Nitroaromatics in Water

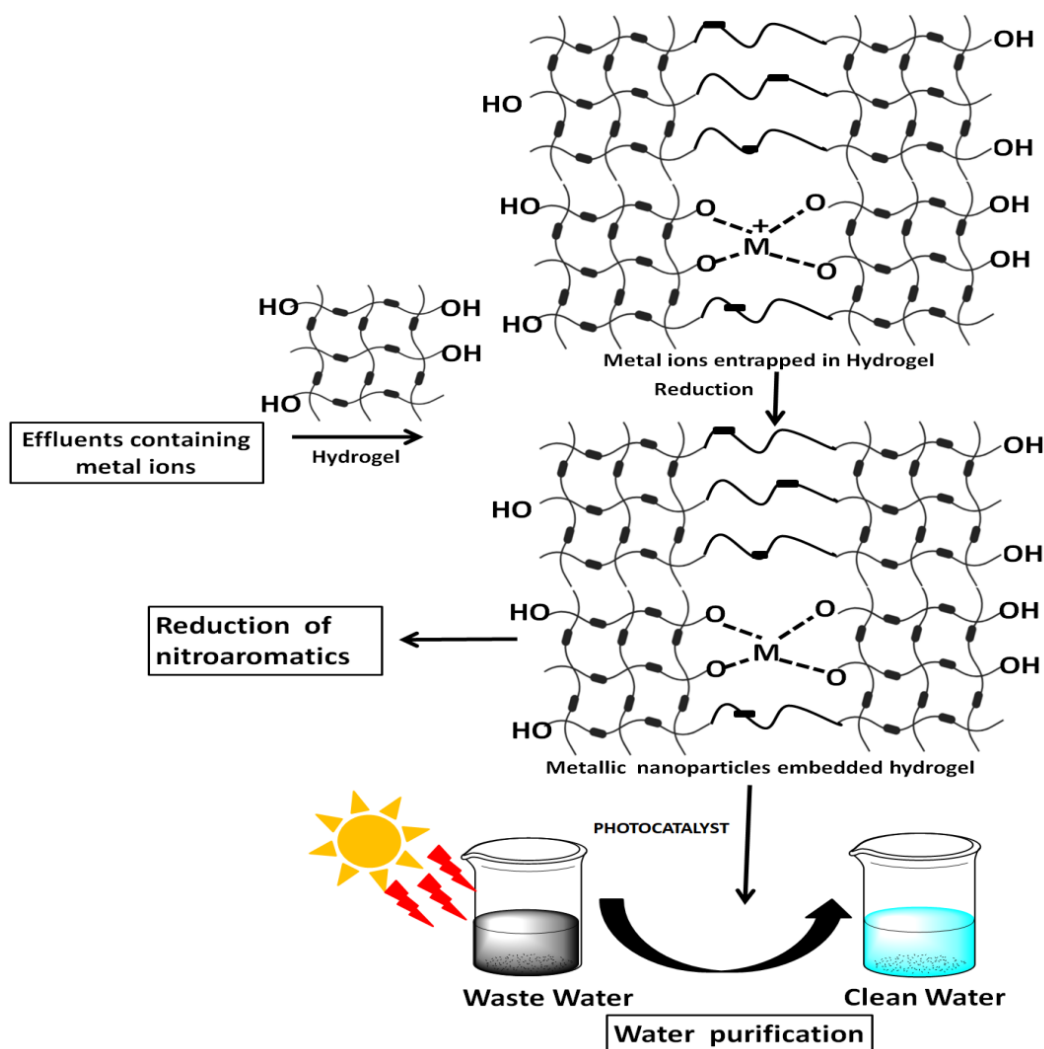


Figure 3.17: Schematic for preparation of valorized metallopolymer Ag@Hydrogel

The effluent from industries also contains precious metal ions as pollutants such as silver, gold, platinum, palladium etc. It is challenging to isolate such metals. A strategy is presented herein (Figure 3.17) not only for the recovery of such metal ions from water, but also for their further utilization as catalyst systems.

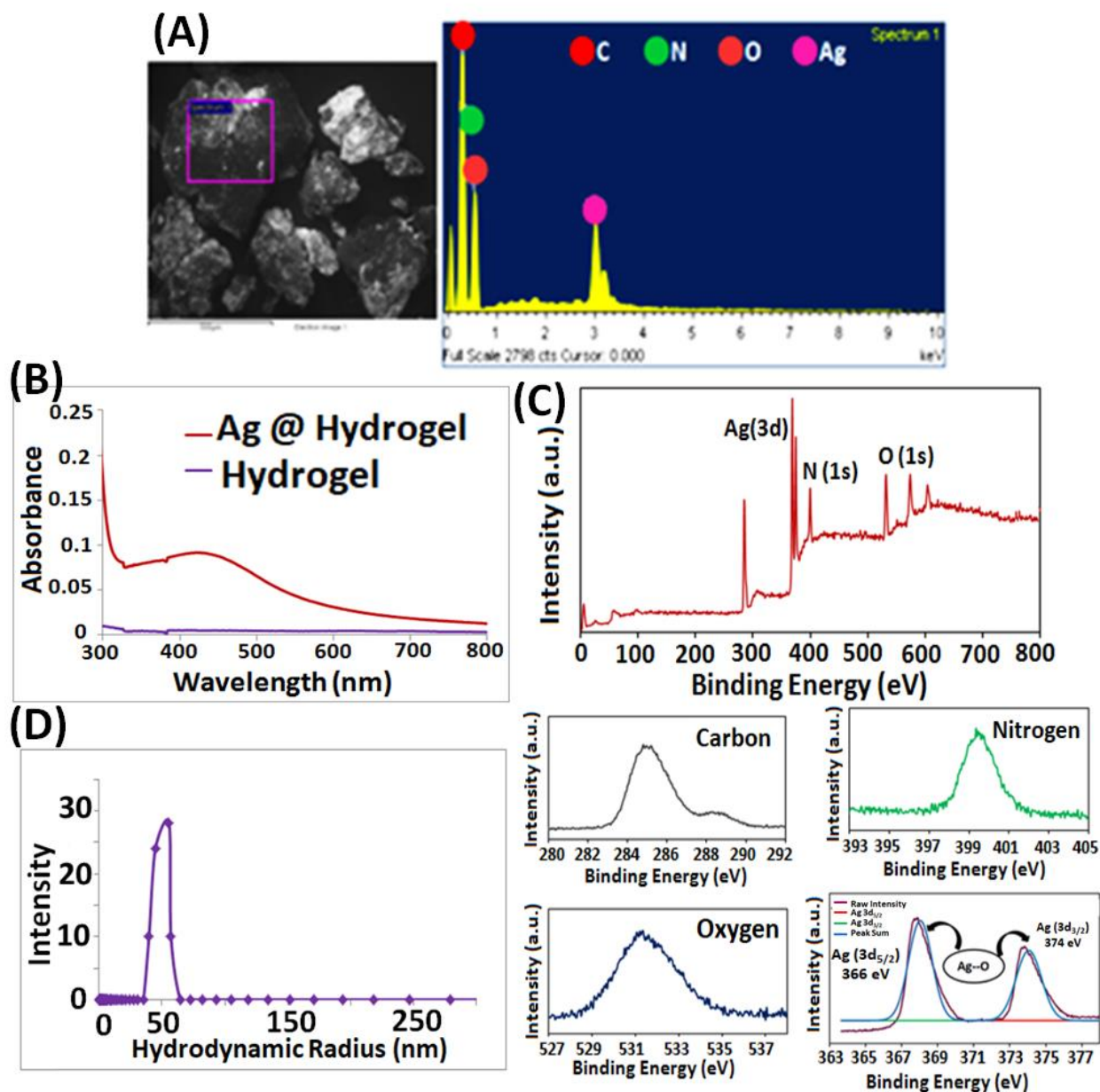


Figure 3.18: Characterizations of valorized metalopolymer (A)SEM image and EDS spectrum showing presence of Ag (B) appearance of SPR band due to formation of Ag nanoparticles observed by UV-vis spectrophotometric determination (C) XPS and (D) DLS spectrum

We selected silver ions as the model expensive metal because it can be easily reduced to nanoparticles. The hydrogel was dispersed in a solution of Ag metal ions after the equilibrium is reached the entrapped silver ions are reduced to silver nanoparticles and hence attain non

toxicity. The content of silver nanoparticles in the vesicles was investigated using EDS mapping (**Figure 3.18 (A)**, **Table 3.5**) and was found to be 10.93 wt%. The appearance of Surface Plasmon Resonance absorption (SPR) band as per **Figure 3.18 (B)** in the region between 400 and 450 nm suggests the reduction of entrapped Ag^+ ions in the hydrogel matrix to Ag nanoparticles⁶⁴. The presence of silver was further confirmed by the XPS analysis. The spectra shown in **Figure 3.18 (C)** depict the presence of the desired elements (C, N, O and Ag) and corroborates with EDX results.

The data as represented in the table suggests the presence of only C, N, O and Ag in the final product as the signals corresponding to other elements were not found. The deconvolution of the peaks corresponding to silver shows (**Figure 3.18 (C)**) the presence of doublet at 366 eV corresponding to $3d_{5/2}$ and at 374 eV corresponding to $3d_{3/2}$ ⁶⁵. The shift towards lower binding energy from 374 eV to 368 eV suggests that interactions exist between O of hydroxyl groups and $\text{Ag}^{65,66}$. The difference in the spin energies amongst the two peaks signifies the presence of Ag in the zerovalent state (Ag^0) thus confirming the formation of nanoparticles in the hydrogel matrix⁶⁷. The hydrodynamic diameter of Ag@Hydrogel as determined using Dynamic Light Scattering (DLS) experiments at 25°C exhibited 55 nm sized monodispersed silver nanoparticles (**Figure 3.18 (D)**). The structure of Ag@Hydrogel was characterized using IR where the peak at 627 cm^{-1} corresponding to Ag-O vibrational bond⁶⁸ was observed along with the presence of other reported peaks of hydrogel. This suggests the attachment of silver to the polymer matrix.

Table 3.5: Elemental Composition of Ag@Hydrogel

Material	C (wt %)	N (wt %)	O (wt %)	Ag (wt %)
Hydrogel	50.67	0	49.33	0
Ag@Hydrogel	43.55	2.99	42.93	10.93

3.3.13. Reduction of Nitroaromatics and Sunlight Mediated Photocatalytic Capability of Ag@Hydrogel

For the assessment of catalytic performance of Ag@Hydrogel the reduction reaction of 4-nitrophenol (4-NP) to 4-aminophenol (p-AP) was selected as a model nitroaromatic reduction reaction. The progress of the reaction was monitored using UV-vis Spectrophotometric determinations (**Figure 3.19**). It was observed that Ag@Hydrogel exhibited excellent catalytic

activity as the conversion of 4-NP to 4-AP occurs in few seconds at much higher concentration of substrate and consuming low amount of reducing agents as compared to other reported systems (**Table 3.6**)²⁴. This conversion is further accelerated in the presence of sunlight. ICP analysis confirmed no leaching of Ag^+ ions from the catalyst on recycling.

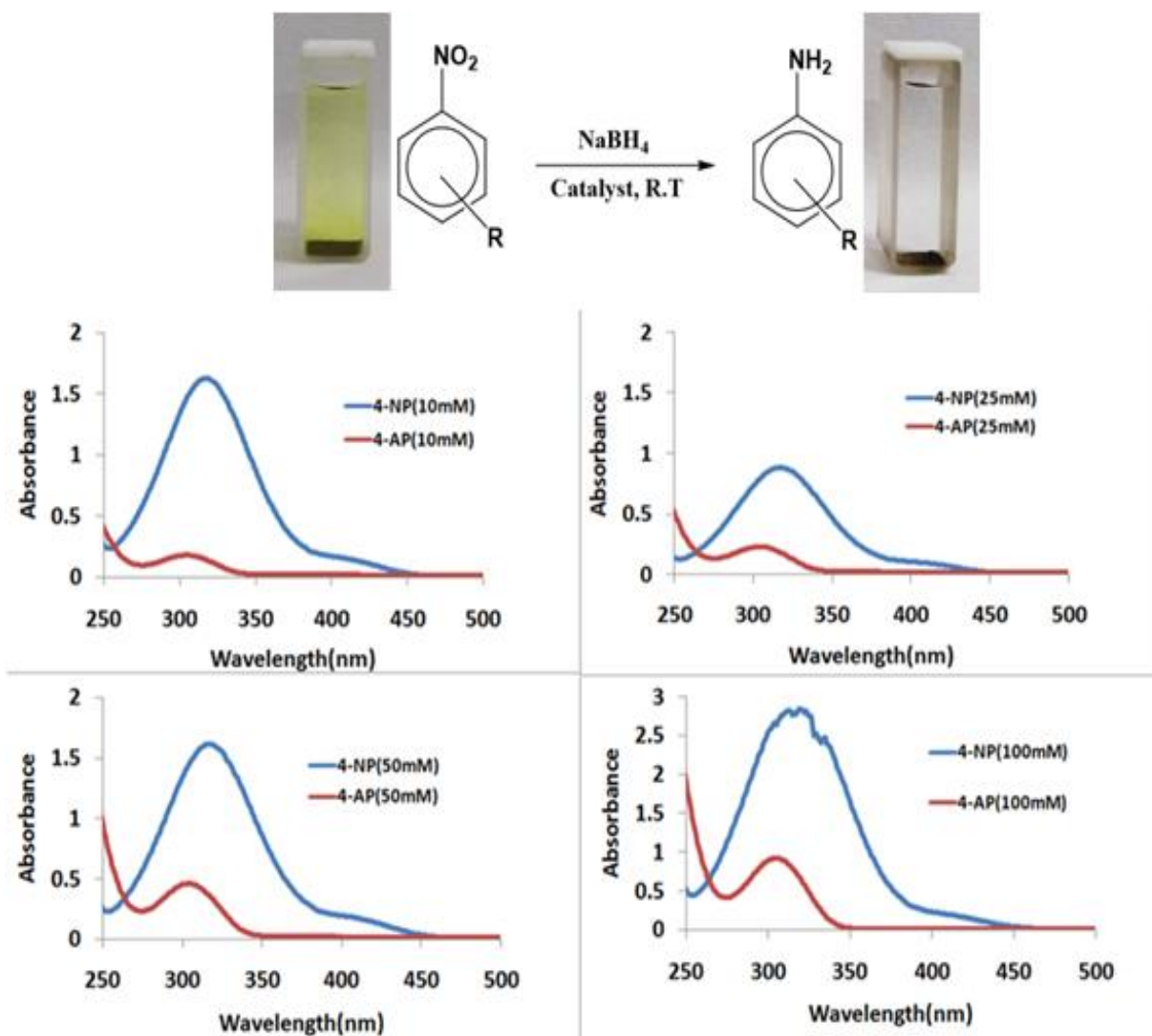


Figure 3.19: General scheme for the reduction of nitroaromatics and UV-vis spectrophotometric determinations for reduction of varying concentrations of 4-NP using Ag@Hydrogel

Table 3.6: Reduction of 4-NP at Different Concentrations using Ag@Hydrogel as Catalyst

Sr.no	Quantity of Ag@hydrogel (mg)	Concentration of 4-Nitrophenol (mM)	Time (s) At room temperature	Time (s) In presence of sunlight
1	10	10	21	10
2		25	55	40
3		50	85	48
4		100	130	52

Reaction conditions: All the reactions were carried using 50 μL of 0.1 M 4-NP, $5 \times 10^{-3}\text{M}$ NaBH_4 .

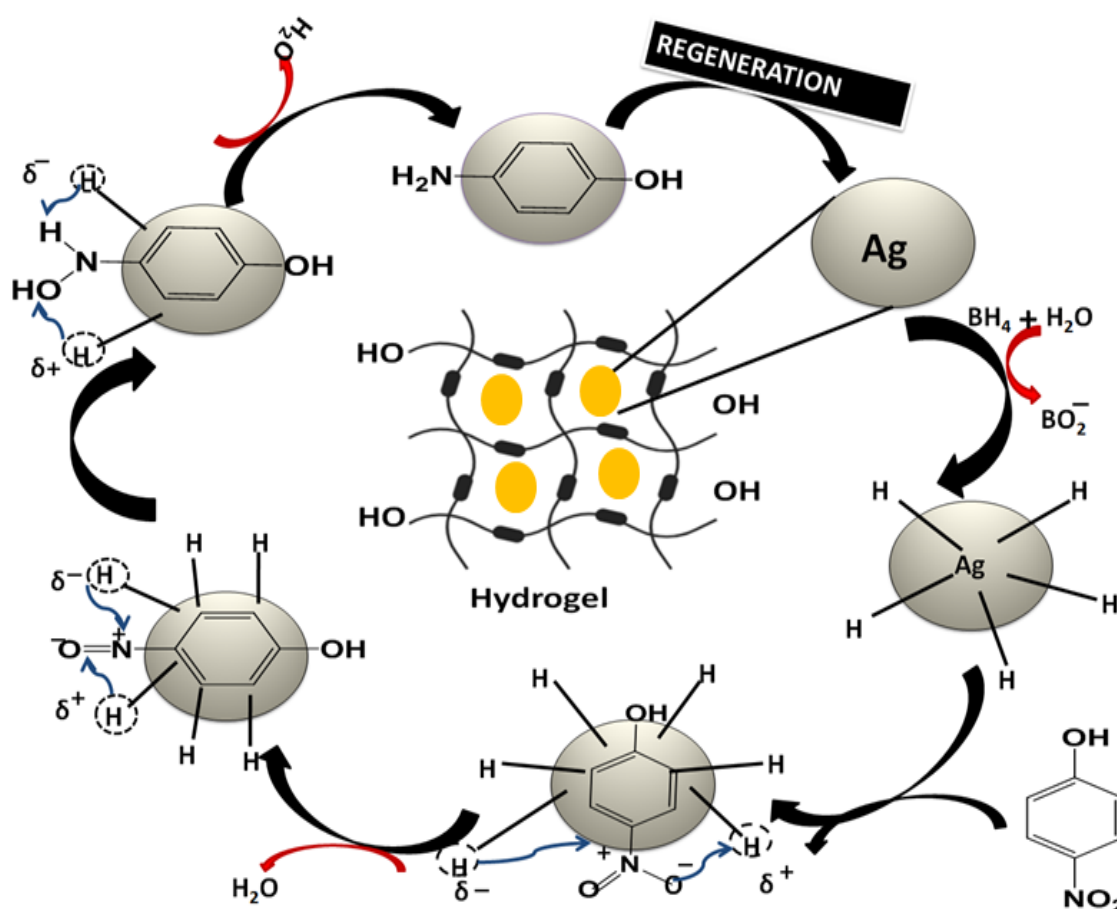


Figure 3.20: Probable mechanism for reduction of 4-NP to 4-NA over valorized catalyst Ag@Hydrogel

The reduction of the nitroaromatics pollutant molecules proceeds via the mechanism of electron transfer and is demonstrated in **Figure 3.20**. The first step involves the adsorption of both 4-NP and sodium borohydride which is the source of hydrogen ions which assists reduction. An enhancement in the reduction upon exposure to sunlight is a result the presence of photo generated electrons. Such photo generated electrons are highly mobile and have increased lifetime due to presence of energetically favored electron-hole separation at interfaces^{64, 69}. The IR spectra corresponding to the recycled Ag@Hydrogel as shown in **Figure 3.21 (A)** represents no change in the characteristic peaks suggesting the hydrogel does not undergo degradation. Ag@Hydrogel shows good catalytic activity upto 5 catalytic cycles (**Figure 3.21 (B)**). The time of reduction gradually increases due to the loss of catalytic sites during the consecutive cycles of reaction. This is due to gradual accumulation of an oxide layer in the process of electron relay from the donor BH_4 to nitrophenolate acceptor ion⁷⁰.

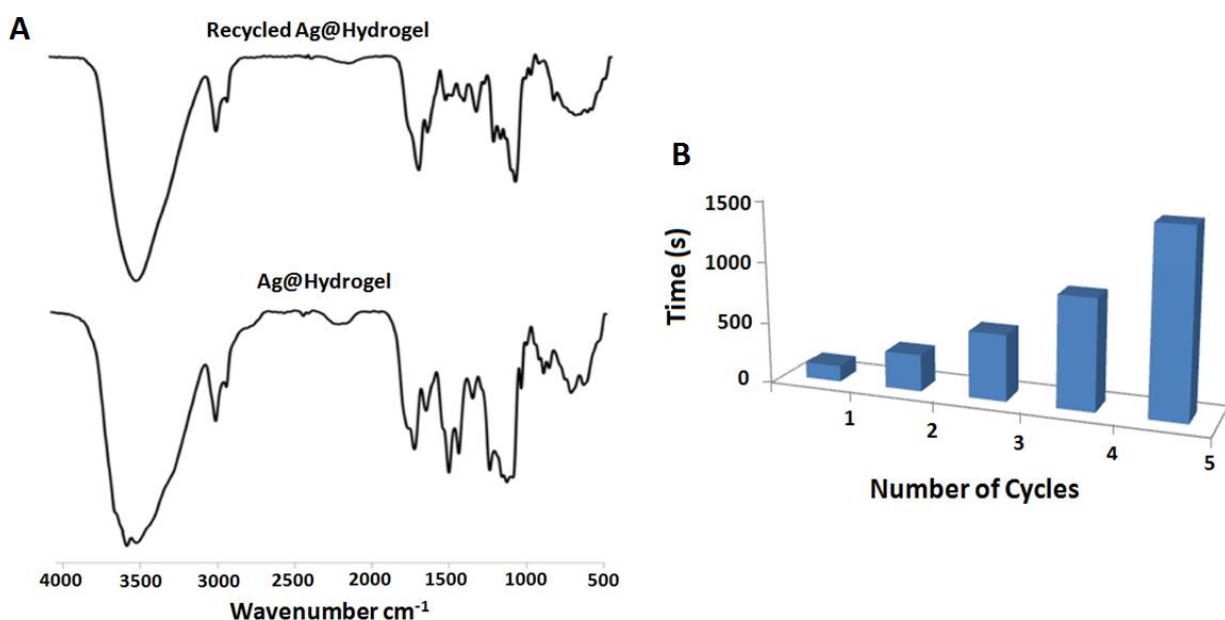


Figure 3.21: (A) FT-IR overlay of fresh and recycled metallopolymer (B) Recycling studies

3.4. Future perspectives for commercialization of hydrogel and remediation on a large scale

The choice of renewable resource as the raw material makes the feedstock handling and process of production economically viable. The process flow diagram for hydrogel production is shown

in **Figure 3.22**. As per the nature of effluents released the ideal site characterized for the practical application of these hydrogels are majorly textile and pharmaceutical industries. The process flow chart for the effluent treatment using the hydrogel is shown in **Figure 3.23**. The valorized metallopolymer can reduce Nitrophenols to Aminophenols which are important starting materials for preparation of antipyretics and analgesics. Thus the reduced product can be further purified and transported for commercial profits. However, engineering validations are required for the selection of most suitable parameters for efficient and feasible functioning of both production and effluent treatment plant.

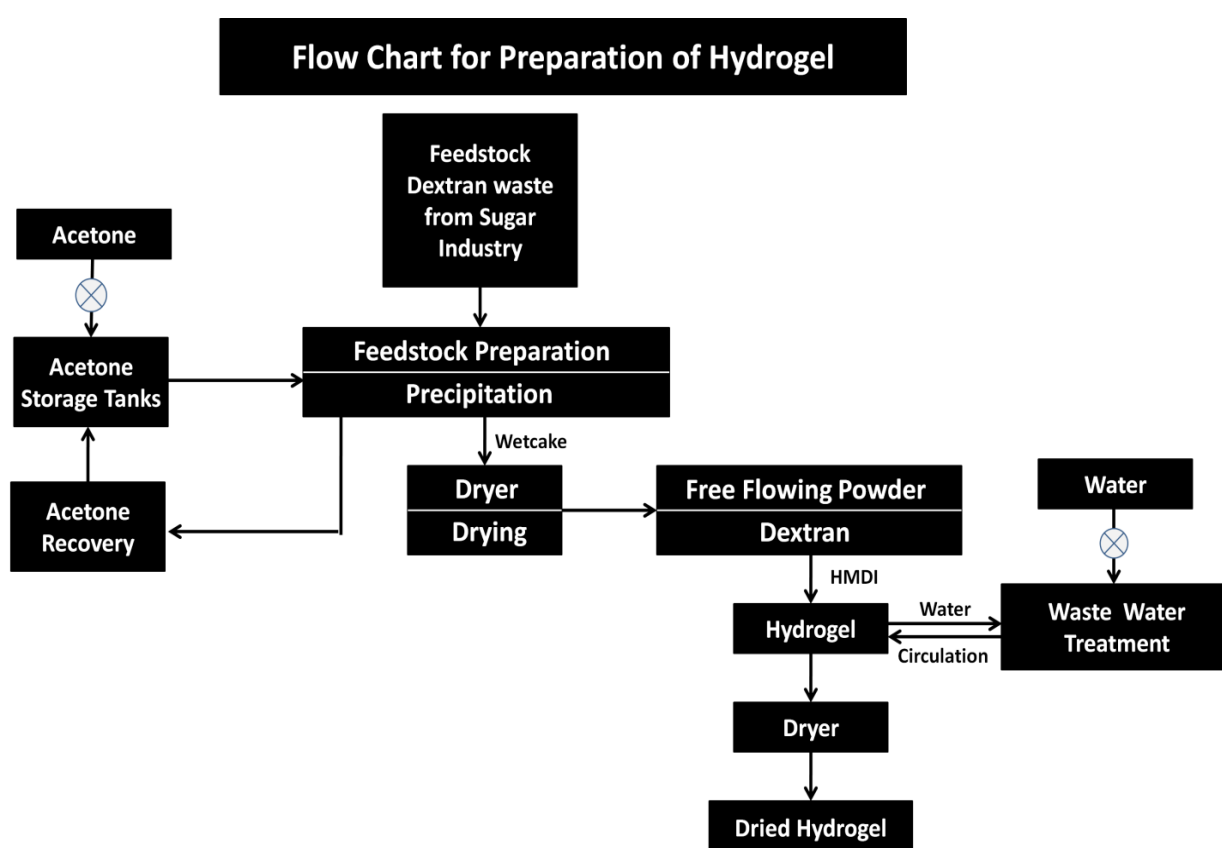


Figure 3.22: Process flow diagram for commercial production of dextran derived Hydrogels

Process Flow for Water Remediation and Value Addition

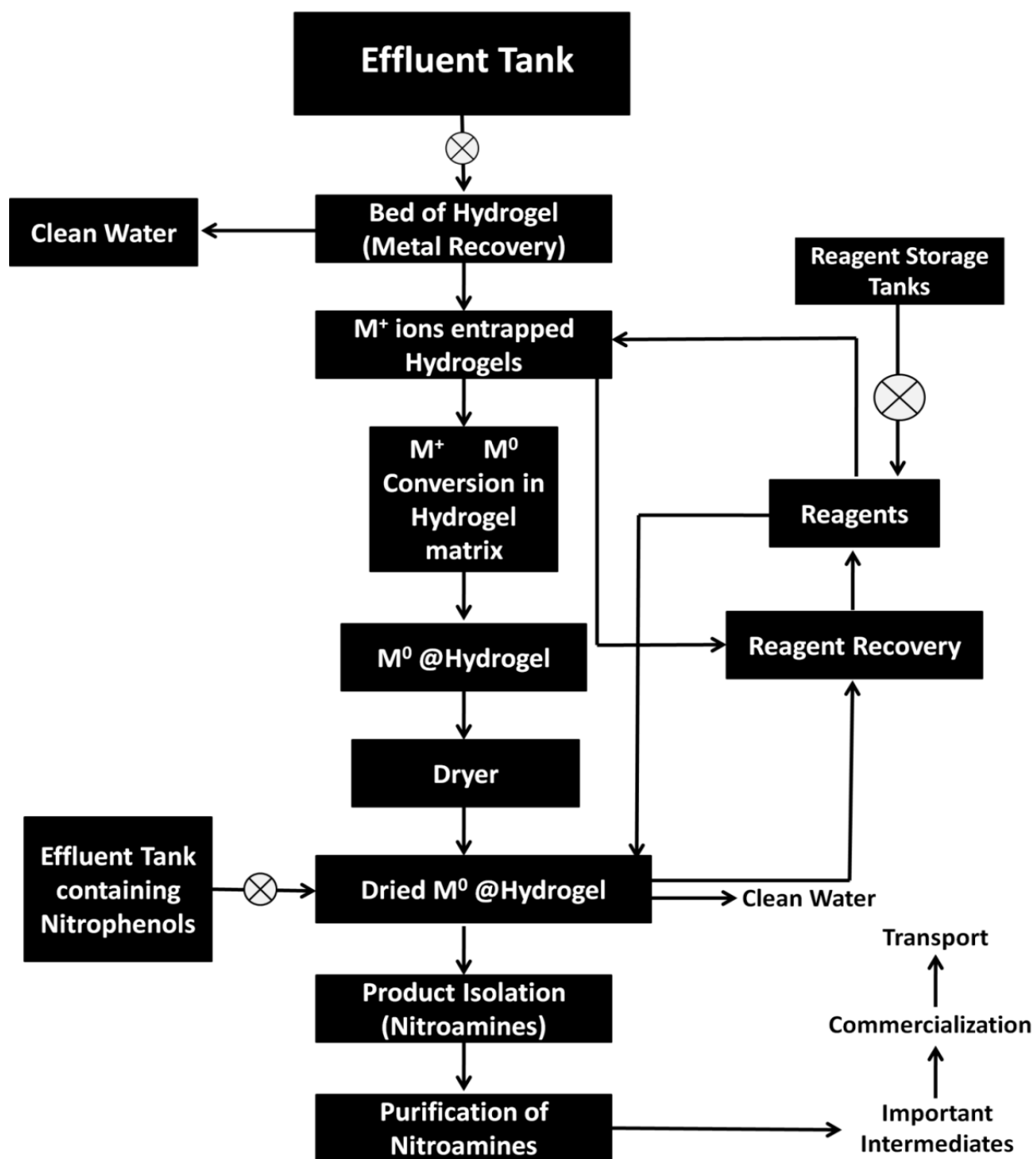


Figure 3.23: Process flow diagram for practical application of Ag@Hydrogel for nitroaromatics reduction

3.5. Conclusions

To summarize, the purpose of our work was to demonstrate a sustainable strategy for using agro wastes in effluent treatment by removal of varied class of co-existing pollutants along with the value addition of used adsorbent. The hydrogel exhibited excellent dye removal efficiency of 84% for MO and 98% for MB. From adsorption isotherms it was observed that, phenomenon of chemisorption occurs with monolayer adsorption on adsorbent surface and follows pseudo second order kinetics. An increase in temperature by 10 °C further enhances the removal by 4%. The thermodynamic studies revealed negative values of Gibbs free energy at all three experimental temperatures. The positive values of entropy ($\Delta S^\circ = 235.43 \text{ J mol}^{-1}$ for MB and 84.66 J mol^{-1} for MO) indicated that adsorption via hydrogel is a spontaneous process. Positive enthalpy values ($\Delta H^\circ = 66618 \text{ J mol}^{-1}$ for MB and 23204 J mol^{-1} for MO) suggested that the process is endothermic in nature. The hydrogel could also efficiently entrap Ag metal ions and the resulting metallopolymer exhibited excellent sunlight mediated photocatalysis, reducing 4-NP to 4-AP in less than 30 seconds. Both the hydrogel and metallopolymer demonstrates efficient recyclability upto 5 cycles. A future outlook for practical applications at large scale has been demonstrated via process flow charts.

References

- (1) Wu, Z.; Zhang, D.; Cai, Y.; Wang, X.; Zhang, L.; Chen, Y. Water Quality Assessment Based on the Water Quality Index Method in Lake Poyang: The Largest Freshwater Lake in China. *Sci. Rep.* **2017**, *7* (1), 1–10. <https://doi.org/10.1038/s41598-017-18285-y>.
- (2) Yadav, M.; Singh, G.; Jadeja, R. N. Bioremediation of Organic Pollutants: A Sustainable Green Approach. In *Sustainable Environmental Clean-up Green Remediation*; Kumar Mishra, V., Kumar, A. B. T.-S. E. C., Eds.; Elsevier, 2021; pp 131–147. <https://doi.org/10.1016/B978-0-12-823828-8.00006-2>.
- (3) Narula, A.; Rao, C. P. Hydrogel of the Supramolecular Complex of Graphene Oxide and Sulfonatocalix[4]Arene as Reusable Material for the Degradation of Organic Dyes: Demonstration of Adsorption and Degradation by Spectroscopy and Microscopy. *ACS Omega* **2019**, *4* (3), 5731–5740. <https://doi.org/10.1021/acsomega.9b00545>.
- (4) Liu, L.; Zhang, B.; Zhang, Y.; He, Y.; Huang, L.; Tan, S.; Cai, X. Simultaneous Removal of Cationic and Anionic Dyes from Environmental Water Using Montmorillonite-Pillared Graphene Oxide. *J. Chem. Eng. Data* **2015**, *60* (5), 1270–1278. <https://doi.org/10.1021/je5009312>.
- (5) Mao, B.; Sidhureddy, B.; Thirupathi, A. R.; Wood, P. C.; Chen, A. Efficient Dye Removal and Separation Based on Graphene Oxide Nanomaterials. *New J. Chem.* **2020**, *44* (11), 4519–4528. <https://doi.org/10.1039/c9nj05895h>.
- (6) Zeng, H.; Lu, W.; Hao, L.; Helms, G. L.; Zhang, Q.; Luo, Z. Adsorptive Removal of P-Nitrophenol from Water with Mechano-Synthesized Porous Organic Polymers. *New J. Chem.* **2018**, *42* (24), 20205–20211. <https://doi.org/10.1039/c8nj04575e>.
- (7) Gu, X.; Kang, H.; Li, H.; Liu, X.; Dong, F.; Fu, M.; Chen, J. Adsorption Removal of Various Nitrophenols in Aqueous Solution by Aminopropyl-Modified Mesoporous MCM-48. *J. Chem. Eng. Data* **2018**, *63* (9), 3606–3614. <https://doi.org/10.1021/acs.jced.8b00477>.
- (8) Hassan, M. M.; Carr, C. M. A Critical Review on Recent Advancements of the Removal of Reactive Dyes from Dyehouse Effluent by Ion-Exchange Adsorbents. *Chemosphere* **2018**, *209*, 201–219. <https://doi.org/10.1016/j.chemosphere.2018.06.043>.
- (9) Amuguni, H.; Mmari, J.; Mwanza, P. Brewers' Spent Grain in Adsorption of Aqueous Congo Red and Malachite Green Dyes: Batch and Continuous Flow Systems. *J. Hazard.*

- Mater.* **2019**, *380*, 120897. <https://doi.org/10.1016/j.jhazmat.2019.120897>.
- (10) Bolisetty, S.; Peydayesh, M.; Mezzenga, R. Sustainable Technologies for Water Purification from Heavy Metals: Review and Analysis. *Chem. Soc. Rev.* **2019**, *48* (2), 409–724. <https://doi.org/10.1039/c8cs00493e>.
- (11) Chen, J.; Chen, H. Removal of Anionic Dyes from an Aqueous Solution by a Magnetic Cationic Adsorbent Modified with DMDAAC. *New J. Chem.* **2018**, *42* (9), 7262–7271. <https://doi.org/10.1039/c8nj00635k>.
- (12) Akpotu, S. O.; Moodley, B. MCM-48 Encapsulated with Reduced Graphene Oxide/Graphene Oxide and as-Synthesised MCM-48 Application in Remediation of Pharmaceuticals from Aqueous System. *J. Mol. Liq.* **2018**, *261*, 540–549. <https://doi.org/10.1016/j.molliq.2018.04.046>.
- (13) Hadi, P.; Guo, J.; Barford, J.; McKay, G. Multilayer Dye Adsorption in Activated Carbons-Facile Approach to Exploit Vacant Sites and Interlayer Charge Interaction. *Environ. Sci. Technol.* **2016**, *50* (10), 5041–5049. <https://doi.org/10.1021/acs.est.6b00021>.
- (14) Guo, D.; Muhammad, N.; Lou, C.; Shou, D.; Zhu, Y. Synthesis of Dendrimer Functionalized Adsorbents for Rapid Removal of Glyphosate from Aqueous Solution. *New J. Chem.* **2019**, *43* (1), 121–129. <https://doi.org/10.1039/c8nj04433c>.
- (15) Rasheed, T.; Adeel, M.; Nabeel, F.; Bilal, M.; Iqbal, H. M. N. TiO₂/SiO₂ Decorated Carbon Nanostructured Materials as a Multifunctional Platform for Emerging Pollutants Removal. *Sci. Total Environ.* **2019**, *688*, 299–311. <https://doi.org/10.1016/j.scitotenv.2019.06.200>.
- (16) Tang, Y.; Yang, R.; Ma, D.; Zhou, B.; Zhu, L.; Yang, J. Removal of Methyl Orange from Aqueous Solution by Adsorption onto a Hydrogel Composite. *Polym. Polym. Compos.* **2018**, *26* (2), 161–168. <https://doi.org/10.1177/096739111802600204>.
- (17) Rajabi, M.; Mahanpoor, K.; Moradi, O. Removal of Dye Molecules from Aqueous Solution by Carbon Nanotubes and Carbon Nanotube Functional Groups: Critical Review. *RSC Adv.* **2017**, *7* (74), 47083–47090. <https://doi.org/10.1039/c7ra09377b>.
- (18) Liu, Q.; Li, Y.; Chen, H.; Lu, J.; Yu, G.; Maxim, M. Superior Adsorption Capacity of Functionalised Straw Adsorbent for Dyes and Heavy-Metal Ions. *J. Hazard. Mater.* **2020**, *382*, 121040. <https://doi.org/10.1016/j.jhazmat.2019.121040>.
- (19) Afkhani, A.; Saber-Tehrani, M.; Bagheri, H. Simultaneous Removal of Heavy-Metal Ions

- in Wastewater Samples Using Nano-Alumina Modified with 2,4-Dinitrophenylhydrazine. *J. Hazard. Mater.* **2010**, *181* (1–3), 836–844. <https://doi.org/10.1016/j.jhazmat.2010.05.089>.
- (20) Chowdhury, A.; Kumari, S.; Khan, A. A.; Hussain, S. Selective Removal of Anionic Dyes with Exceptionally High Adsorption Capacity and Removal of Dichromate ($\text{Cr}_2\text{O}_7^{2-}$) Anion Using Ni-Co-S/CTAB Nanocomposites and Its Adsorption Mechanism. *J. Hazard. Mater.* **2019**, 121602. <https://doi.org/10.1016/J.JHAZMAT.2019.121602>.
- (21) Qi, X.; Wu, L.; Su, T.; Zhang, J.; Dong, W. Polysaccharide-Based Cationic Hydrogels for Dye Adsorption. *Colloids Surfaces B Biointerfaces* **2018**, *170*, 364–372. <https://doi.org/10.1016/j.colsurfb.2018.06.036>.
- (22) Malakootian, M.; Heidari, M. R. Reactive Orange 16 Dye Adsorption from Aqueous Solutions by Psyllium Seed Powder as a Low-Cost Biosorbent: Kinetic and Equilibrium Studies. *Appl. Water Sci.* **2018**, *8* (7), 1–9. <https://doi.org/10.1007/s13201-018-0851-2>.
- (23) Jeon, Y. S.; Lei, J.; Kim, J. H. Dye Adsorption Characteristics of Alginate/Polyaspartate Hydrogels. *J. Ind. Eng. Chem.* **2008**, *14* (6), 726–731. <https://doi.org/10.1016/j.jiec.2008.07.007>.
- (24) Hui, Sun; Jinhui, Jiang; Yufen, X. J. Du. Efficient Removal of PAHs, Dyes and Heavy Metal Ions by a Homopolymer Vesicle. *ACS Appl. Mater. Interfaces* **2017**, *10*, 713–722. <https://doi.org/10.1021/acsami.7b15242>.
- (25) Wang, Y.; Astruc, D.; Abd-El-Aziz, A. S. Metallopolymers for Advanced Sustainable Applications. *Chem. Soc. Rev.* **2019**, *48* (2), 558–636. <https://doi.org/10.1039/c7cs00656j>.
- (26) Potier, J.; Menuel, S.; Fournier, D.; Fourmentin, S.; Woisel, P.; Monflier, E.; Hapiot, F. Cooperativity in Aqueous Organometallic Catalysis: Contribution of Cyclodextrin-Substituted Polymers. *ACS Catal.* **2012**, *2* (7), 1417–1420. <https://doi.org/10.1021/cs300254t>.
- (27) Zhou, Z.; He, C.; Yang, L.; Wang, Y.; Liu, T.; Duan, C. Alkyne Activation by a Porous Silver Coordination Polymer for Heterogeneous Catalysis of Carbon Dioxide Cycloaddition. *ACS Catal.* **2017**, *7* (3), 2248–2256. <https://doi.org/10.1021/acscatal.6b03404>.
- (28) Bhatnagar, A.; Kesari, K. K.; Shurpali, N. Multidisciplinary Approaches to Handling Wastes in Sugar Industries. *Water, Air, Soil Pollut.* **2016**, *227* (1), 1–30.

- <https://doi.org/10.1007/s11270-015-2705-y>.
- (29) Chauhan, M. K.; Varun; Chaudhary, S.; Kumar, S.; Samar. Life Cycle Assessment of Sugar Industry: A Review. *Renew. Sustain. Energy Rev.* **2011**, *15* (7), 3445–3453. <https://doi.org/10.1016/j.rser.2011.04.033>.
- (30) Singh, S.; Shauloff, N.; Jelinek, R. Solar-Enabled Water Remediation via Recyclable Carbon Dot/Hydrogel Composites. *ACS Sustain. Chem. Eng.* **2019**, *7* (15), 13186–13194. <https://doi.org/10.1021/acssuschemeng.9b02342>.
- (31) Zeng, T.; Hu, X. qin; Wu, H.; Yang, J. wen; Zhang, H. bin. Microwave Assisted Synthesis and Characterization of a Novel Bio-Based Flocculant from Dextran and Chitosan. *Int. J. Biol. Macromol.* **2019**, *131*, 760–768. <https://doi.org/10.1016/j.ijbiomac.2019.03.116>.
- (32) Chen, D.; Feng, H.; Li, J. Graphene Oxide: Preparation, Functionalization, and Electrochemical Applications. *Chem. Rev.* **2012**, *112* (11), 6027–6053. <https://doi.org/10.1021/cr300115g>.
- (33) Karousis, N.; Tagmatarchis, N. Current Progress on the Chemical Modification of Carbon Nanotubes. *Chem. Rev.* **2010**, *110*, 5366–5397.
- (34) Hu, X. S.; Liang, R.; Sun, G. Super-Adsorbent Hydrogel for Removal of Methylene Blue Dye from Aqueous Solution. *J. Mater. Chem. A* **2018**, *6* (36), 17612–17624. <https://doi.org/10.1039/c8ta04722g>.
- (35) Kuang, H.; Wu, Y.; Zhang, Z.; Li, J.; Chen, X.; Xie, Z.; Jing, X.; Huang, Y. Double PH-Responsive Supramolecular Copolymer Micelles Based on the Complementary Multiple Hydrogen Bonds of Nucleobases and Acetalated Dextran for Drug Delivery. *Polym. Chem.* **2015**, *6* (19), 3625–3633. <https://doi.org/10.1039/c5py00042d>.
- (36) Zhou, Q.; Feng, F.; Yang, Y.; Zhao, F.; Du, R.; Zhou, Z.; Han, Y. Characterization of a Dextran Produced by *Leuconostoc Pseudomesenteroides* XG5 from Homemade Wine. *Int. J. Biol. Macromol.* **2018**, *107*, 2234–2241. <https://doi.org/10.1016/j.ijbiomac.2017.10.098>.
- (37) Li, R. H.; Zhang, H. bin; Hu, X. Q.; Gan, W. W.; Li, Q. P. An Efficiently Sustainable Dextran-Based Flocculant: Synthesis, Characterization and Flocculation. *Chemosphere* **2016**, *159*, 342–350. <https://doi.org/10.1016/j.chemosphere.2016.06.010>.
- (38) Sun, Y.; Zhu, C.; Sun, W.; Xu, Y.; Xiao, X.; Zheng, H.; Wu, H.; Liu, C. Plasma-Initiated Polymerization of Chitosan-Based CS-g-P(AM-DMDAAC) Flocculant for the Enhanced Flocculation of Low-Algal-Turbidity Water. *Carbohydr. Polym.* **2017**, *164*, 222–232.

- <https://doi.org/10.1016/j.carbpol.2017.02.010>.
- (39) Das, M.; Solanki, A.; Joshi, A.; Devkar, R.; Seshadri, S. β -Cyclodextrin Based Dual-Responsive Multifunctional Nanotheranostics for Cancer Cell Targeting and Dual Drug Delivery. *Carbohydr. Polym.* **2019**, *206*, 694–705. <https://doi.org/10.1016/j.carbpol.2018.11.049>.
- (40) Singha, N. R.; Mahapatra, M.; Karmakar, M.; Dutta, A.; Mondal, H.; Chattopadhyay, P. K. Synthesis of Guar Gum-: G-(Acrylic Acid-Co-Acrylamide-Co-3-Acrylamido Propanoic Acid) IPN via in Situ Attachment of Acrylamido Propanoic Acid for Analyzing Superadsorption Mechanism of Pb(II)/Cd(II)/Cu(II)/MB/MV. *Polym. Chem.* **2017**, *8* (44), 6750–6777. <https://doi.org/10.1039/c7py01564j>.
- (41) Pirgalioglu, S.; Özbelge, T. A.; Özbelge, H. Ö.; Bıcak, N. Crosslinked PolyDADMAC Gels as Highly Selective and Reusable Arsenate Binding Materials. *Chem. Eng. J.* **2015**, *262*, 607–615. <https://doi.org/10.1016/j.cej.2014.10.015>.
- (42) Dinu, M. V.; Dinu, I. A.; Lazar, M. M.; Dragan, E. S. Chitosan-Based Ion-Imprinted Cryo-Composites with Excellent Selectivity for Copper Ions. *Carbohydr. Polym.* **2018**, *186*, 140–149. <https://doi.org/10.1016/j.carbpol.2018.01.033>.
- (43) Xu, X.; Bai, B.; Ding, C.; Wang, H.; Suo, Y. Synthesis and Properties of an Ecofriendly Superabsorbent Composite by Grafting the Poly(Acrylic Acid) onto the Surface of Dopamine-Coated Sea Buckthorn Branches. *Ind. Eng. Chem. Res.* **2015**, *54* (13), 3268–3278. <https://doi.org/10.1021/acs.iecr.5b00092>.
- (44) Qi, X.; Hu, X.; Wei, W.; Yu, H.; Li, J.; Zhang, J.; Dong, W. Investigation of Salecan/Poly(Vinyl Alcohol) Hydrogels Prepared by Freeze/Thaw Method. *Carbohydr. Polym.* **2015**, *118*, 60–69. <https://doi.org/10.1016/j.carbpol.2014.11.021>.
- (45) Yadav, M.; Das, M.; Savani, C.; Thakore, S.; Jadeja, R. Maleic Anhydride Cross-Linked β -Cyclodextrin-Conjugated Magnetic Nanoabsorbent: An Ecofriendly Approach for Simultaneous Adsorption of Hydrophilic and Hydrophobic Dyes. *ACS Omega* **2019**, *4*, 11993–12003. <https://doi.org/10.1021/acsomega.9b00881>.
- (46) Qi, X.; Wei, W.; Su, T.; Zhang, J.; Dong, W. Fabrication of a New Polysaccharide-Based Adsorbent for Water Purification. *Carbohydr. Polym.* **2018**, *195*, 368–377. <https://doi.org/10.1016/j.carbpol.2018.04.112>.
- (47) Yang, X.; Ni, L. Synthesis of Hybrid Hydrogel of Poly(AM Co DADMAC)/Silica Sol and

- Removal of Methyl Orange from Aqueous Solutions. *Chem. Eng. J.* **2012**, *209*, 194–200. <https://doi.org/10.1016/j.cej.2012.07.123>.
- (48) Yang, X.; Li, Y.; Du, Q.; Sun, J.; Chen, L.; Hu, S.; Wang, Z.; Xia, Y.; Xia, L. Highly Effective Removal of Basic Fuchsin from Aqueous Solutions by Anionic Polyacrylamide/Graphene Oxide Aerogels. *J. Colloid Interface Sci.* **2015**, *453*, 107–114. <https://doi.org/10.1016/j.jcis.2015.04.042>.
- (49) Li, D.; Li, Q.; Bai, N.; Dong, H.; Mao, D. One-Step Synthesis of Cationic Hydrogel for Efficient Dye Adsorption and Its Second Use for Emulsified Oil Separation. *ACS Sustain. Chem. Eng.* **2017**, *5* (6), 5598–5607. <https://doi.org/10.1021/acssuschemeng.7b01083>.
- (50) Das, S.; Dash, S. K.; Parida, K. M. Kinetics, Isotherm, and Thermodynamic Study for Ultrafast Adsorption of Azo Dye by an Efficient Sorbent: Ternary Mg/(Al + Fe) Layered Double Hydroxides. *ACS Omega* **2018**, *3*, 2532–2545. <https://doi.org/10.1021/acsomega.7b01807>.
- (51) Azmier, M.; Azreen, N.; Puad, A.; Solomon, O. Kinetic, Equilibrium and Thermodynamic Studies of Synthetic Dye Removal Using Pomegranate Peel Activated Carbon Prepared by Microwave-Induced KOH Activation. *Water Resour. Ind.* **2014**, *6*, 18–35. <https://doi.org/10.1016/j.wri.2014.06.002>.
- (52) Yan, L.; Lv, M.; Su, C.; Zheng, L.; Li, J.; Ye, Z. An Efficient Supramolecular Adsorbent for Co-Adsorption of Dyes and Metal Ions from Wastewater and Its Application in Self-Healing Materials. *Soft Matter* **2017**, *13* (46), 8772–8780. <https://doi.org/10.1039/c7sm01977g>.
- (53) Yang, D.; Qiu, L.; Yang, Y. Efficient Adsorption of Methyl Orange Using a Modified Chitosan Magnetic Composite Adsorbent. *J. Chem. Eng. Data* **2016**, *61* (11), 3933–3940. <https://doi.org/10.1021/acs.jced.6b00706>.
- (54) Liu, Y.; Luo, C.; Sun, J.; Li, H.; Sun, Z.; Yan, S. Enhanced Adsorption Removal of Methyl Orange from Aqueous Solution by Nanostructured Proton-Containing δ -MnO₂. *J. Mater. Chem. A* **2015**, *3* (10), 5674–5682. <https://doi.org/10.1039/c4ta07112c>.
- (55) Sharifpour, E.; Haddadi, H.; Ghaedi, M.; Asfaram, A.; Wang, S. Simultaneous and Rapid Dye Removal in the Presence of Ultrasound Waves and a Nano Structured Material: Experimental Design Methodology, Equilibrium and Kinetics. *RSC Adv.* **2016**, *6* (70), 66311–66319. <https://doi.org/10.1039/c6ra13286c>.

- (56) Stanciu, M. C.; Nichifor, M. Adsorption of Anionic Dyes on a Cationic Amphiphilic Dextran Hydrogel: Equilibrium, Kinetic, and Thermodynamic Studies. *Colloid Polym. Sci.* **2019**, *297* (1), 45–57. <https://doi.org/10.1007/s00396-018-4439-z>.
- (57) Mahida, V. P.; Patel, M. P. Removal of Some Most Hazardous Cationic Dyes Using Novel Poly (NIPAAm/AA/N-Allylisatin) Nanohydrogel. *Arab. J. Chem.* **2016**, *9* (3), 430–442. <https://doi.org/10.1016/j.arabjc.2014.05.016>.
- (58) Omid, S.; Kakanejadifard, A. Eco-Friendly Synthesis of Graphene-Chitosan Composite Hydrogel as Efficient Adsorbent for Congo Red. *RSC Adv.* **2018**, *8* (22), 12179–12189. <https://doi.org/10.1039/c8ra00510a>.
- (59) Pourjavadi, A.; Nazari, M.; Kabiri, B.; Hosseini, S. H.; Bennett, C. Preparation of Porous Graphene Oxide/Hydrogel Nanocomposites and Their Ability for Efficient Adsorption of Methylene Blue. *RSC Adv.* **2016**, *6* (13), 10430–10437. <https://doi.org/10.1039/c5ra21629j>.
- (60) Fan, J.; Shi, Z.; Lian, M.; Li, H.; Yin, J. Mechanically Strong Graphene Oxide/Sodium Alginate/Polyacrylamide Nanocomposite Hydrogel with Improved Dye Adsorption Capacity. *J. Mater. Chem. A* **2013**, *1* (25), 7433–7443. <https://doi.org/10.1039/c3ta10639j>.
- (61) Mahmoud, G. A.; Mohamed, S. F.; Hassan, H. M. Removal of Methylene Blue Dye Using Biodegradable Hydrogel and Reusing in a Secondary Adsorption Process. *Desalin. Water Treat.* **2015**, *54* (10), 2765–2776. <https://doi.org/10.1080/19443994.2014.905978>.
- (62) Kundu, D.; Mondal, S. K.; Banerjee, T. Development of β - Cyclodextrin-Cellulose / Hemicellulose-Based Hydrogels for the Removal of Cd (II) and Ni (II): Synthesis , Kinetics , and Adsorption Aspects. *J. Chem. Eng. Data* **2019**, *64*, 2601–2617. <https://doi.org/10.1021/acs.jced.9b00088>.
- (63) Zhang, H.; Omer, A. M.; Hu, Z.; Yang, L. Y.; Ji, C.; Ouyang, X. kun. Fabrication of Magnetic Bentonite/Carboxymethyl Chitosan/Sodium Alginate Hydrogel Beads for Cu (II) Adsorption. *Int. J. Biol. Macromol.* **2019**, *135*, 490–500. <https://doi.org/10.1016/j.ijbiomac.2019.05.185>.
- (64) Ravichandran, V.; Vasanthi, S.; Shalini, S.; Shah, S. A. A.; Tripathy, M.; Paliwal, N. Green Synthesis, Characterization, Antibacterial, Antioxidant and Photocatalytic Activity of Parkia Speciosa Leaves Extract Mediated Silver Nanoparticles. *Results Phys.* **2019**, *15*, 102565. <https://doi.org/10.1016/j.rinp.2019.102565>.

- (65) Aditya, T.; Jana, J.; Singh, N. K.; Pal, A.; Pal, T. Remarkable Facet Selective Reduction of 4-Nitrophenol by Morphologically Tailored (111) Faceted Cu₂O Nanocatalyst. *ACS Omega* **2017**, *2* (5), 1968–1984. <https://doi.org/10.1021/acsomega.6b00447>.
- (66) Aditya, T.; Jana, J.; Pal, A.; Pal, T. One-Pot Fabrication of Perforated Graphitic Carbon Nitride Nanosheets Decorated with Copper Oxide by Controlled Ammonia and Sulfur Trioxide Release for Enhanced Catalytic Activity. *ACS Omega* **2018**, *3* (8), 9318–9332. <https://doi.org/10.1021/acsomega.8b00968>.
- (67) Gu, S.; Wunder, S.; Lu, Y.; Ballauff, M.; Fenger, R.; Rademann, K.; Jaquet, B.; Zaccone, A. Kinetic Analysis of the Catalytic Reduction of 4-Nitrophenol by Metallic Nanoparticles. *J. Phys. Chem. C* **2014**, *118* (32), 18618–18625. <https://doi.org/10.1021/jp5060606>.
- (68) Ma, Y. F.; Wang, L. J.; Zhou, Y. L.; Zhang, X. X. A Facile Synthesized Glutathione-Functionalized Silver Nanoparticle-Grafted Covalent Organic Framework for Rapid and Highly Efficient Enrichment of N-Linked Glycopeptides. *Nanoscale* **2019**, *11* (12), 5526–5534. <https://doi.org/10.1039/c9nr00392d>.
- (69) Ibrahim, I.; Athanasekou, C.; Manolis, G.; Kaltzoglou, A.; Nasikas, N. K.; Katsaros, F.; Devlin, E.; Kontos, A. G.; Falaras, P. Photocatalysis as an Advanced Reduction Process (ARP): The Reduction of 4-Nitrophenol Using Titania Nanotubes-Ferrite Nanocomposites. *J. Hazard. Mater.* **2019**, *372*, 37–44. <https://doi.org/10.1016/j.jhazmat.2018.12.090>.
- (70) Nariya, P.; Das, M.; Shukla, F.; Thakore, S. Synthesis of Magnetic Silver Cyclodextrin Nanocomposite as Catalyst for Reduction of Nitro Aromatics and Organic Dyes. *J. Mol. Liq.* **2020**, *300*, 112279. <https://doi.org/10.1016/j.molliq.2019.112279>.

Published Paper from this Chapter:

NJC



PAPER

Cite this: *New J. Chem.*, 2020, 44, 19122

Facile design of a dextran derived polyurethane hydrogel and metallopolymer: a sustainable approach for elimination of organic dyes and reduction of nitrophenols†

Manita Das,^a Monika Yadav,^b Falguni Shukla,^a Sagufa Ansari,^a R. N. Jadeja^{ab} and Sonal Thakore^{ab*}

This work reports a sustainable approach for fabrication of a highly cost-effective and operation-convenient adsorbent derived from dextran and its valorization to a metallopolymer photocatalyst. The hydrogel with a significant magnitude of equilibrium water absorbency (EWA) was prepared by crosslinking with hexamethylene diisocyanate in a simple one pot synthesis. Due to numerous functionalities, the hydrogel not only adsorbs cationic and anionic dyes but also efficiently scavenges heavy and valuable metal ions from effluents. The removal efficiency of dyes (concentration 100 mg L⁻¹) is greater than 80% in the presence of 100 mg of adsorbent. The adsorption process and its probable mechanism are supported by both experimental (via appropriate analytical characterization) and theoretical (kinetic modelling and thermodynamic calculations) evidence. The recovery of heavy metals was demonstrated with silver ions, which were further readily reduced to silver nanoparticles to generate a metallopolymer photocatalyst. The latter catalyzes complete reduction of nitrophenol within 10 seconds in the presence of sunlight. A process flow diagram for commercial scale up and production of an economically viable adsorbent for effluent treatment using waste from the sugar industry and its valorization as a photocatalyst is reported for the first time.

Received 14th April 2020,
Accepted 17th October 2020

DOI: 10.1039/d0nj01871f

rsc.li/njc

1. Introduction

The release of hazardous pollutants due to anthropogenic activities and the subsequent deterioration of water quality is a serious concern being faced globally.¹ Water with a poor WQI (water quality index) is unfit for usage and hampers the health and economic development of a country. Amongst various classes of pollutants the removal of harmful organics like dyes and phenolic compounds from water requires attention. The presence of dyes eluted from printing, dyeing, textile and chemical industries can have adverse impacts on the quality of drinking water, thus posing serious threats to living beings.^{2–4} Nitrophenols on the other hand are released as effluents from oil refineries, the pharmaceutical industry,

petrochemical plants⁵ etc. and are strongly irritating substances possessing the risk of causing liver and kidney damage.⁶ Several approaches taken up for the removal of such pollutants include physical techniques such as adsorption, irradiation and membrane processes, chemical processes like oxidation, ozonation, ionic exchange, electrocoagulation, and coagulation-flocculation and various biological methods.^{7,8} Some of these methods despite being effective are associated with shortcomings like use of expensive chemicals having potential for bioaccumulation and expensive technologies for remediation.⁹ Considering these facts, adsorption can be considered to be the most convenient and cost effective technique for effluent treatment.¹⁰ Over the past few years various adsorbent materials like activated carbon,¹¹ MCM,¹² graphene oxide,² mesoporous SiO₂,¹³ dendrimers,¹⁴ carbon nanotubes,¹⁵ polymer-clay,¹⁶ alumina,¹⁷ agricultural waste,¹⁸ bio-adsorbents,¹⁹ nano-adsorbents,²⁰ hydrogels²¹ etc. have been developed with the aim of pollutant removal and have shown good adsorption properties. Amongst all these adsorbents, hydrogels composed of a three-dimensional network of hydrophilic polymers have shown high adsorption capacities due to a controllable swelling property and the ability to hold a large amount of water while maintaining their structure.²² These studies however are focused on elimination

^a Department of Chemistry, Faculty of Science, The Maharaja Sayajirao University of Baroda, Vadodara 390 002, India. E-mail: drsonalit@gmail.com, chemistry2797@yahoo.com

^b Department of Environmental Studies, Faculty of Science, The Maharaja Sayajirao University of Baroda, Vadodara 390 002, India

^c Institute of Interdisciplinary Studies, The Maharaja Sayajirao University of Baroda, Vadodara 390 002, India

† Electronic supplementary information (ESI) available. See DOI: 10.1039/d0nj01871f